Role of the Composition of Cyclohexane-extracted gangue on its drying at ambient conditions

by

Reza Khalkhali

A thesis submitted in partial fulfillment of the requirements for the degree of

Master of Science

in

Chemical Engineering

Department of Chemical and Materials Engineering

University of Alberta

Abstract

Non-aqueous extraction (NAE) of bitumen from oil sands has recently regained interest as a replacement for the commercial, water-based extraction method. NAE has the potential to alleviate all the current water-induced extraction challenges such as high fresh water consumption, high heat consumption and carbon emissions, and the issue of ever-growing tailing ponds. Recovery of solvent from the "gangue," the mixture of solids, connate water, residual bitumen, and residual solvent (cyclohexane in this study) after the extraction, is the biggest environmental and economical challenge of NAE.

Drying of the gangue, like any other porous materials, consists of two general stages: the initial cyclohexane-dominated stage with a fast, constant, and linear drying rate and the final water-dominated stage which is almost an order of magnitude slower compared to the initial stage. The fast, constant drying rate of the initial stage is due to the presence of "liquid cyclohexane film flow" which occurs in the corners of pores as a result of capillary forces being dominant over viscous and gravity forces. The dominance of capillary forces is also demonstrated in this work through the estimation of capillary and Bond numbers developed for a square pore channel.

The initial stage of drying consists of two processes: liquid transfer by film flow to the top surface of the drying bed and evaporation through a diffuse layer from the surface. Measurements of evaporation flux showed that it is much slower (approximately two orders of magnitude) than the film flow rate which is estimated using a model developed for a square pore channel.

To study the effect of gangue's composition on its initial drying rate, different sets of gangue samples with controlled compositions were artificially prepared and they are called "reconstituted gangue." Drying of various reconstituted gangue samples with different bituminous carbon (Bit.C), water, and fine solids (solid particles <45µm) content were studied. Moreover, to further investigate the role of water on cyclohexane liquid film formation, the drying of different samples with 1 M solution of NaCl as well as n-butanol instead of water were also studied. The effect of each component on the initial drying rate was explained by its effect(s) on the film flow rate.

Increasing Bit.C content from 0.0 to only 1.0 wt% remarkedly decreased the initial drying rate (more than 30%) by increasing the viscosity of cyclohexane/bitumen solution. Bitumen can also significantly contribute to cyclohexane retention by absorbing an equilibrium concentration of cyclohexane.

Increasing water content from 6 to 12 wt% significantly slowed down the initial drying stage by more than 60%, while completely removing water also resulted in slower initial drying rate compared to samples with 3.88 and 6.0 wt% water. The role of water was explained by looking into the pore saturation by water and cyclohexane. Water content higher than a certain amount starts to fully cover the solid's surface, not allowing the formation of cyclohexane liquid films. Moreover, the lower initial drying rate as a result of removing water can be related to a cyclohexane liquid film with a lower average thickness. Moreover, adding NaCl to water had almost no effect on drying. However, replacing water with n-butanol resulted in a much slower initial drying rate. Like the effect of bitumen, this was attributed to the reduction in viscosity due the miscibility of n-butanol and cyclohexane.

Increasing fines content had no significant effect on the initial drying rate. This was unexpected since samples with higher fines content have a smaller mean pore size and thus were expected to show a lower initial drying rate. However, the samples with higher fines contents showed higher hydrophobicity and consequently, higher affinity to cyclohexane which is in favor of film flow rate. Higher hydrophobicity of samples with higher fines is attributed to the much higher carbon content of fines compared to that of coarse solids.

To my beloved family

My parents for their unlimited love and support throughout the ups and downs

And my brother, my third parent, and my best friend, Dr. Mohammad Khalkhali for always inspiring me and making all of this possible.

Acknowledgment

I would like to thank my supervisor, Dr. Phillip Choi, for his continuous guidance and support. I consider myself to have been privileged to work under Dr. Choi's supervision. I learned a lot from my discussions with Dr. Choi not only about my research project but also on how to investigate an academic matter with a "researcher's mind." His meticulous and deep attention to the fundamentals and theoretical backgrounds has always been a source of inspiration to me.

I would also like to thank the Institute for Oil Sands Innovation (IOSI) for providing the lab equipment. I am extremely thankful to the wonderfully helpful IOSI staff, the lab coordinator, Ms. Lisa Brandt, and the lab manager, Dr. Xiaoli Tan for all the lab equipment setups, trainings, and assistance provided during this project.

Finally, I would like to thank the Future Energy Systems (FES) for funding this project.

Table of Contents

List of Figures

List of Tables

1.Introduction

With proven reserves of about 165 billion barrels , Alberta's oil sands is the third largest oil reserves in the world, after Venezuela and Saudi Arabia [1]. Alberta's oil sands underlines 142,000 km^2 of land and is mainly present in three areas: Athabasca, Cold Lake, and Peace River with Athabasca reserves being the largest of the three [2]. About 3% of the oil sands area consisting of 20% of all oil sands reserves is mineable, the rest being too deep (more than 75 m) for mining applications thus extracted by in-situ methods [3], [4]. In the year 2018, more than 3 million barrels of crude bitumen was produced in Alberta. Open mining accounted for about 48% of the production, the rest 52% produced by in-situ processes [5].

1.1. Current Commercial Extraction Processes

There are two main methods for bitumen extraction: in-situ methods and open-pit mining. Although the two are different in their processes and applications, they both use water either in the form of steam or hot liquid water.

1.1.1. In-situ Methods

In-situ methods are used to recover bitumen that lies too deep beneath the surface when mining is not economically viable. Approximately 80% of all oil sands in Alberta fall into this category [3]. Currently, there are two major commercial in-situ methods. In Cyclic Steam Stimulation (CSS), high-pressure high-temperature steam is injected into a vertical well in the oil sands deposit. The high pressure steam cracks into the oil sands formation, heats bitumen, and drops its viscosity allowing it to flow into a producing well, from which it is pumped to the surface [6]. In Steam

Assisted Gravity Drainage (SAGD), two horizontal wells are drilled into the oil sands deposit. High pressure high temperature steam is injected into the top well in order to heat bitumen and reduce its viscosity. The flowing bitumen drains with condensed steam into the lower well, from which it is pumped to the surface [2] (Figure 1).

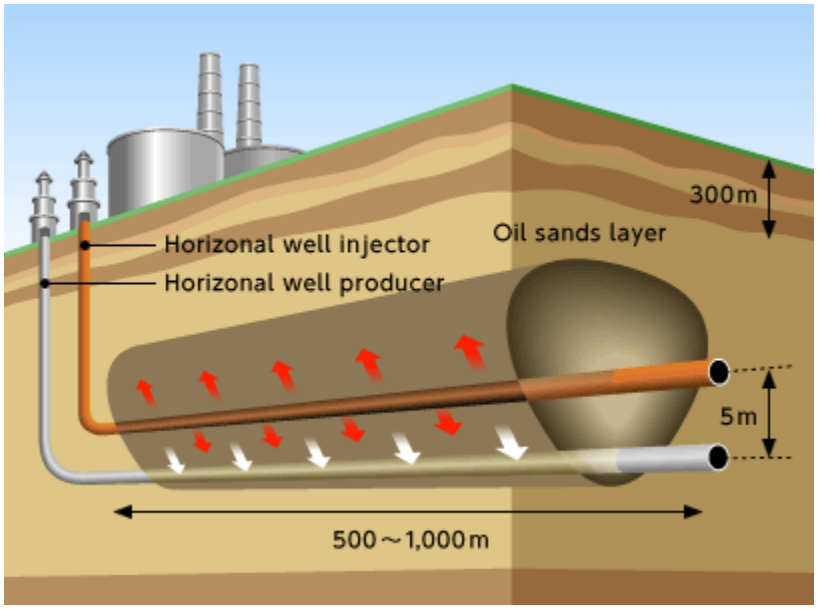

Figure 1- A schematic of SAGD process [7]

Shortcomings of in-situ methods are high carbon gas emissions and low recovery. A study in 2010 found that carbon emission per barrel of oil extracted by SAGD was 19% higher than the U.S. average, while the emissions per barrel of oil produced by mining operations was only 1% higher [8]. Moreover, recovery rates of in-situ techniques are usually less than 60% [5]. There have been efforts to enhance recovery rates of in-situ techniques such as injecting a mixture of steam and a solvent [9]. However, the recovery of the solvent from the reservoir is a major concern.

1.1.2. Surface Mining

For deposits less than 75 m below ground, oil sands ores are surface-mined and processed by hot water. First proposed by Dr. Karl Clark in 1929, the Clark hot water extraction (CHWE) is still the basis for bitumen extraction in commercial plants, although some of the operating parameters have been modified through the years [10].

In this process, the mined ore is crushed and then mixed with a hot basic water-based solution. The high temperature drops bitumen's viscosity while the high pH changes the surface charge and interfacial tensions of bitumen and solids, leading to "liberation" of bitumen from solids' surface in the form of droplets [2]. The liberated bitumen droplets either engulf or attach to air bubbles, generated from forced aeration into the mixture, and float to the top of the vessel where they are collected as bitumen froth [2]. The froth is then treated by an either naphthenic or paraffinic solvent, while the rest of the mixture, i.e., basic alkaline water, solids, and unrecovered bitumen, is discharged to tailing ponds [2].

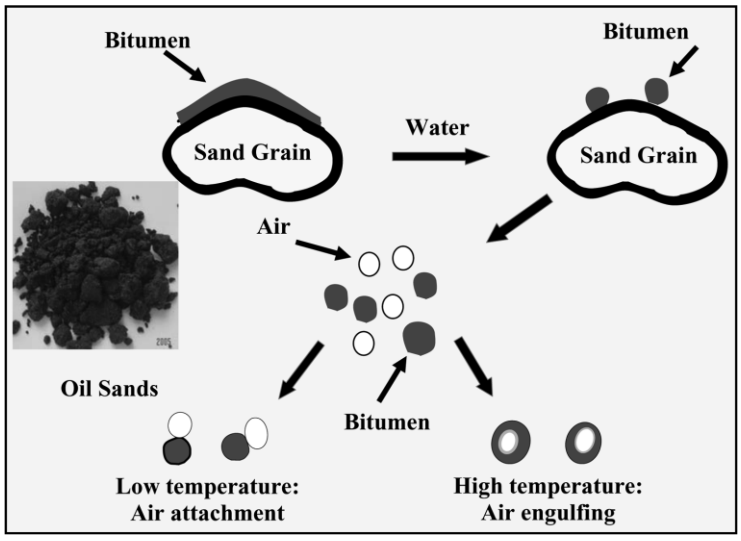

Figure 2- Hot water extraction methods use hot water to "liberate" bitumen from solids surface[11]

CHWE-based methods have been successfully applied on an industrial scale for decades, achieving recovery rates as high as 95%. However, there are some major economic and environmental drawbacks to these methods, all of which arise from the usage of water in the process.

1.2. Drawbacks of CHWE Methods

1.2.1. Fresh Water Intake

Although most of the water used for extraction is recycled back into the extraction process, there is an amount of unrecoverable water trapped in the beaches and fluid fine tailings of tailing ponds which needs to be made up with intake of fresh water [10]. About 3-4 barrels of makeup water are needed for each barrel of synthetic crude bitumen [12]. Fresh water intake from the river, especially during the low flow season, could adversely affect the ecosystem and threaten the aquatic life [10].

1.2.2. Tailing Ponds

The fast and constant growing of tailing ponds has become a major environmental concern. As mentioned before, tailings from CHWE processes contain a mixture of solids, unrecovered bitumen, and alkaline water. Tailings are considered toxic, containing inorganic salts as well as dissolved organic compounds in an alkaline aqueous solution, and therefore cannot be discharged into a water body or ground surface [13]. The clay particles in water are fully dispersed and thermodynamically stable forming the so-called “Fluid Fine Tailings” (FFT), which remains in fluid state indefinitely unless treated [2]. As of to date, the FFT have been accumulated to about

1 billion m^3 and is predicted to double by 2030, should no significant improvement occur regarding tailings treatments [13].

1.2.3. Energy Consumption and GHG Emissions

CHWE-based methods are quite energy intensive. This is due to the extensive amount of thermal energy needed to warm up a considerable amount of water. To produce one barrel of bitumen, about 16 barrels (~2.5 m^3) of water is used to prepare the slurry [10]. To achieve a slurry operation temperature of 40-50 °C, water is added to the crushed ore in high temperatures, i.e., 70-90 °C [2]. This results in spending 1.3 GJ to produce one barrel of upgraded bitumen. This is approximately 20% of equivalent energy within a barrel of bitumen [2].

Oil sands mining also causes high greenhouse gasses emissions, ~ 44 kg of equivalent carbon dioxide (CO_2-e) per each barrel of bitumen produced [10]. In 2014, this translated to the release of about 16 million MT CO_2-e , given the annual production of 365 million barrels from mine operations during that year [14].

1.2.4. Impractical for Low-grade Ores or Oil-wetted Ores

The key to CHWE success in achieving higher than 90% bitumen recovery rates from Athabasca oil sands is the ores' water-wettability which facilitates the liberation of bitumen from solids surface [2]. However, this method has shown to result in poor froth quality and recovery rates as low as 60% for water-wetted low-grade ores, i.e., ores with low bitumen contents and high proportions of fines [2]. In addition, CHWE methods are also considered impractical for oil-wetted ores such as Indonesian oil sands and result in poor recovery rates [15].

1.3. Non-aqueous Extraction

Non-aqueous extraction (NAE) — also known as solvent extraction — is a potentially alternative extraction method. In this method, a non-aqueous solvent is used to "dissolve" bitumen rather than "liberating" it from the solid surface. It can be performed at room temperature and ambient pressure, and result in high extraction rates as bitumen dissolves in most organic solvents [16]. In addition, since water is not used, the tailings that NAE leaves behind— the so-called "gangue" — contains little amount of water which was connately present in the ore. Moreover, bitumen recovery in NAE has shown to be much less affected by ore grades compared to CHWE [17]. Therefore, NAE offers a promising solution to the aforementioned issues of water-based extraction by alleviating all water-induced problems, while resulting in high bitumen recovery rates from a range of ores [18], [19].

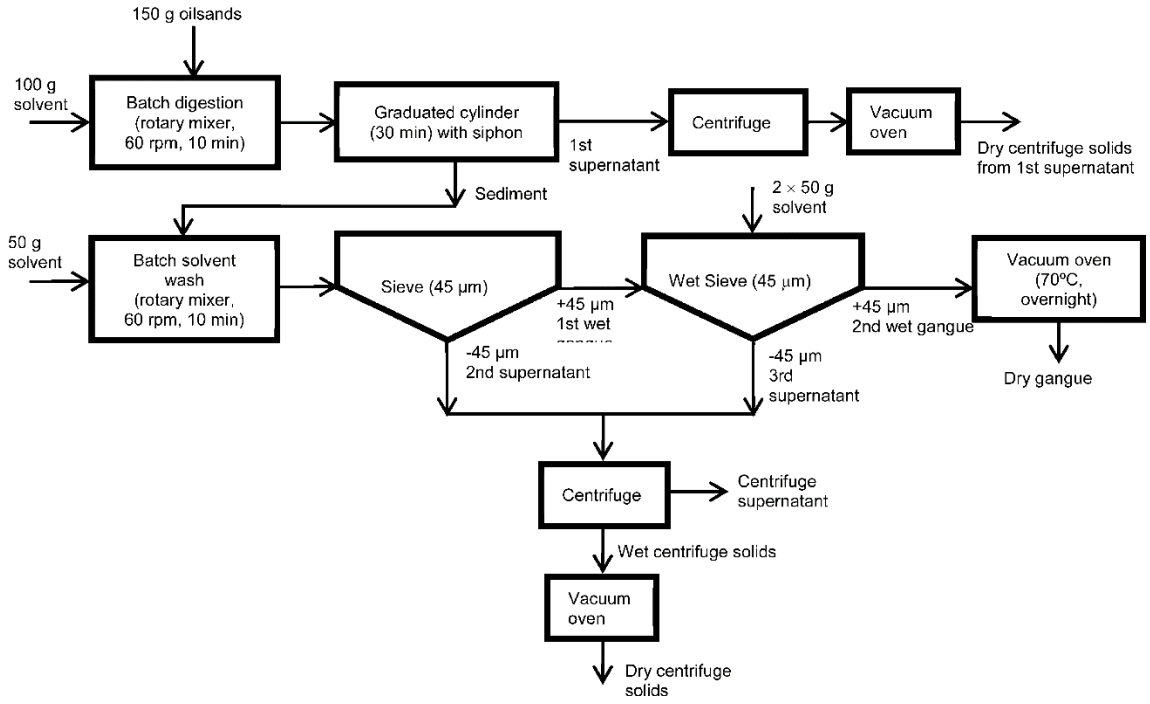

Figure 3- Schematic flow diagram of a lab-scale NAE extraction[20]

Although NAE is not a new concept and the discussion over it started decades ago, it has never been implemented on a fully industrial scale [10]. However, the recently raising concerns over the environmental impacts of tailing ponds and water usage by CHWE methods has renewed interests toward NAE and the possibility of practically applying it on an industrial scale. In order to be a viable replacement to CHWE, NAE processes should employ much lower energy consumption and also minimize water usage, while maintain a high recovery rate of bitumen and leave minor environmental footprints behind [16]. To this end, three major goals need to be achieved: high bitumen recovery rate at room temperature and ambient pressure, high bitumen quality i.e., low fines and emulsified water in the final bitumen product, and maximum solvent recovery from the gangue.

1.3.1. Selection of Solvent

The solvent used for extraction has the most crucial role in addressing the challenges of an NAE process. A "good" solvent for an NAE process [16] has the following characteristics:

- Has high solubility of bitumen, resulting in high extraction rates
- Is not too volatile at operating conditions, so the loss of solvent during extraction can be controlled
- Does not transfer high quantities of fines (solid particles with sizes <44 μm) into the final bitumen product
- Is volatile enough, so the removal of residual solvent from the gangue after the extraction does not require extensive amount of energy

Solvent selection is even more challenging since further criteria regarding the solvent, such as its environment and safety impacts (toxicity) as well as its economic cost, also need to be taken into consideration.

The solvation power of a solvent is determined by solubility parameter. Hildebrand solubility parameter, first described by Hildebrand and Scott [21], is a measure of cohesive energy density and is given by

$$\delta_T = e_{coh}^{\frac{1}{2}} = \left(\frac{\Delta H^{vap} - RT}{V}\right)^{\frac{1}{2}} \quad (1)$$

where δ_T is the Hildebrand solubility parameter, e_{coh} the cohesive energy density, ΔH^{vap} the heat of vaporization, R the gas constant, T the absolute temperature, and V the molar volume.

If the difference between the solubility parameters of the solvent and the solute is small, they will mix as the enthalpy of mixing will be small

$$\Delta H_{mix} = V_m . \Phi_s . \Phi_a (\delta_s - \delta_a)^2 \quad (2)$$

Here, ΔH_{mix} is the mixing enthalpy, V_m the molar volume of the solution, and Φ_s and Φ_a are the volume fractions of the solvent and solute, respectively, and δ_s and δ_a are the solubility parameters of the solvent and solute, respectively.

Rahimian and Zenke attempted to predict bitumen solubility by screening 76 liquid solvents [22]. It was claimed that any good solvent for bitumen has a Hildebrand solubility parameter between

15.3 and 23$MPa^{1/2}$. However, not all liquids with solubility parameter in that range dissolve bitumen [17]. This is due to the fact that Hildebrand solubility parameter only takes into account dispersion forces and therefore, its prediction for systems with certain molecular interactions other than dispersion forces is inaccurate.

Hansen solubility parameter [23] is a more practical measure of cohesive energy as it considers more interactions: dispersion (δ_D), polarity (δ_P), and hydrogen bonding (δ_H)

$$\delta_T^2 = \delta_D^2 + \delta_P^2 + \delta_H^2 \quad (3)$$

Using Heithaus titration, Redelius [17] showed that, unlike Hildebrand solubility parameter, Hansen solubility parameter can accurately predict the solubility behavior of bitumen. Nikakhtari et al. [16] screened 13 solvents, including alkanes, cycloalkanes, aromatics, and biologically derived solvents, and their blends (to achieve different solubility parameters) and investigated their performance in terms of bitumen recovery, bitumen product quality, and residual bitumen in the gangue. Except limonene and isoprene, all the other solvents showed a bitumen recovery of 95% or higher. Fine solids content in the extracted bitumen as the measure of bitumen product quality, was directly correlated to the solubility parameter of the solvent. Fines content in bitumen was below 2.9 wt% (based on extracted bitumen) for all solvents with solubility parameters over 16.5 $MPa^{1/2}$. The efficiency of solvent recovery from the gangue was found to be directly correlated to solvent's vapor pressure which is a measure of solvent's volatility. Finally, cyclohexane was recommended as the best candidate for non-aqueous extraction of Alberta oil sands. It showed a 95% bitumen recovery and 1.4 wt% of fines in extracted bitumen.

In terms of solvent recovery, the residual amount of cyclohexane was only 5 mg/kg of tailings after 60 min of drying in ambient conditions. This was the best drying result after isoprene (which had a weak extraction performance). The solvent used in this study was cyclohexane, accordingly.

1.3.2. Solvent Recovery from the Gangue

Solvent removal from the gangue (solvent-wetted solids after the extraction) is the major technical, economic, safety, and environmental challenge of solvent extraction processes [18], [19]. Before discharging the gangue back to the mining area, the residual solvent content in the gangue needs to be minimized. This is not only to avoid the release of the organic solvent to the environment, but also to make the NAE process economically viable since almost any of organic solvents suitable for extraction is costlier than bitumen itself [18]. The only regulation regarding allowable amount of solvent loss in the tailings is attributed to tailings of froth treatment in hot water extraction which allows up to 4 volumes of solvent loss per 1000 volumes of bitumen produced [2]. Companies have achieved a solvent loss of 3 volumes of solvent loss per 1000 volumes of bitumen so far [16]. This has been the basis for studies on solvent removal from solvent extraction gangue and translates to about 260 mg of residual solvent/1 kg of gangue, i.e. a solvent mass concentration of 260 ppm in the gangue, for a medium grade ore with 10 wt% bitumen [16],[24].

Different approaches have been proposed for solvent removal from the gangue. Methods such as surfactant solution washing [25]–[28] or using a second solvent [29]–[31] seem to add more complication to the problem. This is due to the fact that washing the gangue with a surfactant solution involves introducing water to the mixture which is against one of the very reasons why

NAE processes are favorable. Moreover, washing with a surfactant solution is most effective for high levels of contamination by the organic solvent [32]–[35]. The resulted solution after washing also needs to be treated for maximal recovery of solvent. On the other hand, using a second solvent to help dislodge the original extraction solvent creates solids wetted with another solvent that also needs to be removed. The second solvent should have a low boiling point, so its removal takes a minimum amount of energy [10]. It also should be noted that energy-intensive methods such as steam and gas stripping [36]–[38] or fluidized bed drying [39]–[41] are better to be avoided as much as possible since the energy efficiency of NAE is one of its main advantages over hot water extraction. Although, NAE will only be as energy efficient as hot water extraction even if solvent removal is achieved only through simply heating up the gangue. A comparison of the energy efficiency of the two methods is presented in Appendix A.

Drying the gangue at ambient conditions seems promising regarding both removal and recovery of solvent. Solvents with higher vapor pressure, i.e., being more volatile, generally result in higher recovery rates [16],[42]. However, it is difficult to control the loss of a very volatile solvent during extraction. Therefore, there is a trade-off between solvent's volatility and extraction performance.

As mentioned before, cyclohexane has shown to be a good candidate for solvent extraction, having a rather high vapor pressure (10.33 KPa at 20 °C)[43] compared to all other solvents with acceptable extraction performances [16], [24], [42].

1.4. Drying of Porous Media

Drying of a cyclohexane-extracted gangue at room temperature and ambient pressure provides an example of isothermal drying of two immiscible liquid phases (cyclohexane and water) in a porous solid matrix [44]. The gangue after extraction is a mixture of porous clay/sand solids, a low concentration of residual bitumen which could not be extracted, a significant amount of solvent, and a low amount of water which was connately present in the initial oil sands ore and forms an immobile phase in the presence of organic solvent [42].

1.4.1. Liquid Films on the Drying of Porous Media

Drying in porous media involves displacement of the evaporating fluid by a non-wetting gas/air [45]. According to Yiotis et al. [46], a porous media can be considered to be a network of pores connected to each other by throats. Prior to [46], drying was modeled as the gas-liquid interface remaining immobile until the pressure difference between the two pores exceeds the capillary pressure. Once this happens, the interface recedes instantly due to the assumptions of null throat volume [47]. However, in realistic pore geometries, the displacement of meniscus (gas-liquid interface) is followed by the formation of liquid films along the surface of the pore volume [46] (Figure 4).

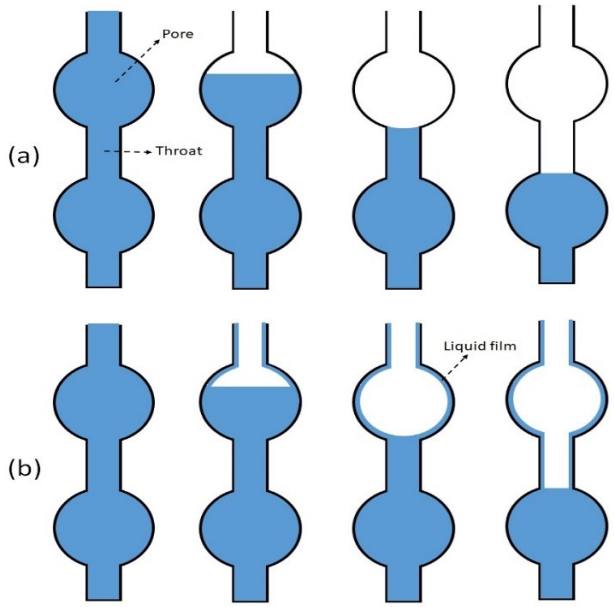

Figure 4- A 2-D visualization of pore-throat network model. Drying of the network (a) without considering liquid film formation (b) with considering liquid film (real case)

Thick films are formed when some of the liquid, which has high affinity for the solid surface, is trapped by capillarity in the corners of polygonal-shaped pore walls after invasion of the pore bulk by the gas phase [48] (Figure 5). The much faster evaporation in channels with corners compared to channels with circular cross sections (presented in [49]) is another proof for the existence of liquid films and their role as the major mechanism for evaporation [48]. It should be noted that the irregular polygonal shape of pores occurs due to the polydisperse shape and size of solid particles. For simplicity, pores will be visualized as channels with square cross sections in this work.

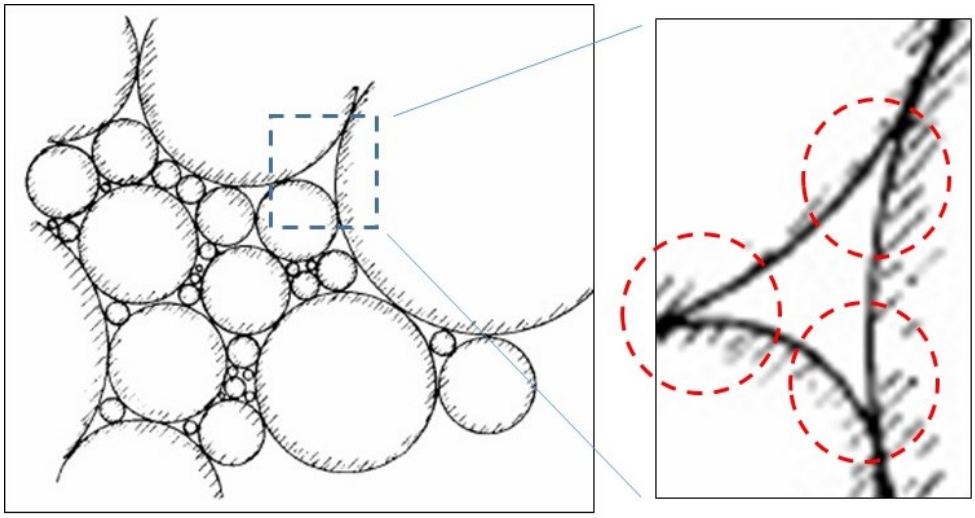

Figure 5 – The pores that occur in a porous material made up of polydisperse spherical particles tend to have corners where liquid films could form

Yiotis et al. [46] developed a rigorous model of a porous network to investigate the role of liquid films on drying. They started by looking at one throat with a square cross-section. The capillary pressure of the liquid film, assuming local capillary equilibrium, is given by the well-known Young-Laplace equation

$$P_c = P_g - P_l \approx -P_l \sim \frac{-\gamma}{r} \quad (4)$$

Where γ and r are respectively the interfacial tension and the radius of curvature, a function of time and distance from the evaporating surface. Since the liquid pressure drops due to fluid flow, there will be a decreasing gradient of radius of curvature in the liquid film, as it gets closer to the top of the sample bed (the open end) (Figure 6). Another factor in establishing this gradient is the faster evaporation of the liquid in the regions closer to the top.

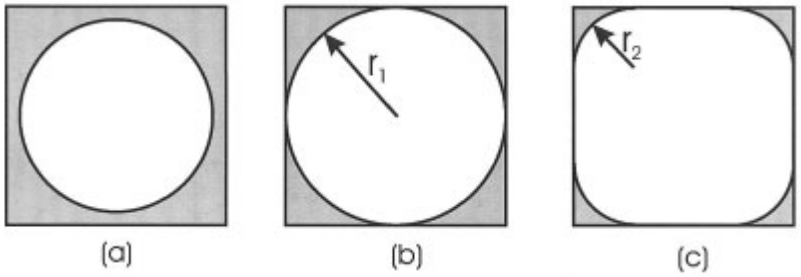

Figure 6- Evolution of the liquid film curvature in a channel with square cross section (top view) [46]*; getting closer to the evaporating surface, from left to right, the radius of curvature decreases, inducing a pressure difference.*

This leads to an upward (toward the open end) capillary flow induced by the difference in the capillary pressure along the liquid film which pumps up the liquid to the surface where it evaporates with a rate close to that of free liquid evaporation (Figure 7). As a result, a constant high evaporation rate is achieved as long as the liquid film connectivity exists.

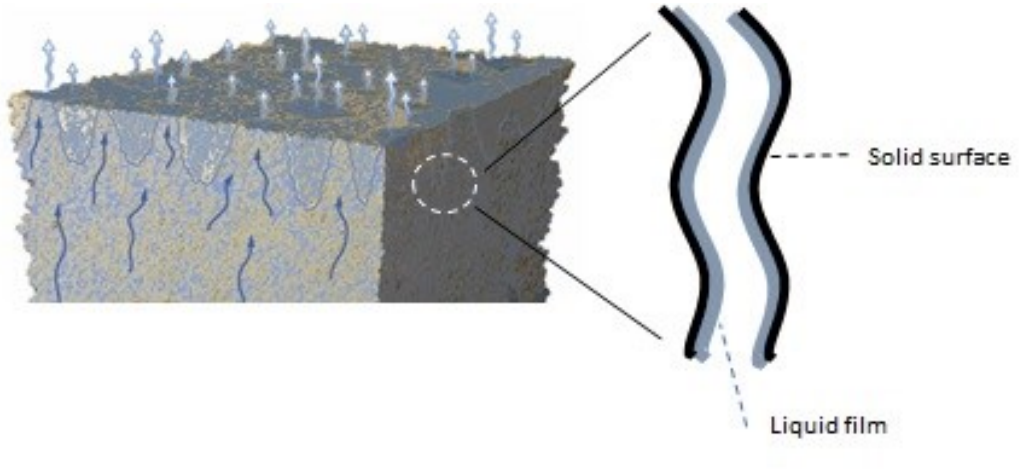

Figure 7 - Formation of the liquid film on solid surface and the upward capillary flow which transfers liquid to the open evaporating surface where it can evaporate with a rate close to that of steady state evaporation

Yiotis et al. [46] characterized this capillary flow (in a throat with square cross-section) using a Poiseuille-type law, assuming unidirectional viscous flow

$$Q_x = -\frac{\alpha . r^4}{\mu_l} . \frac{\partial P_l}{\partial x} \quad (5)$$

where Q_x is the volumetric flow rate, α is a dimensionless geometric factor, and μ_l is the liquid viscosity. Incorporating eq. 4 into eq. 5, leads to

$$Q_x = -\frac{\alpha.\gamma.r^2}{\mu_l}.\frac{\partial r}{\partial x} \quad (6)$$

Moreover, along their derivation, Yiotis et al. [46] defined a dimensionless capillary number as

$$Ca = \frac{\pi D C_e \mu_l}{2\alpha\rho_l r_0 \gamma} \quad (7)$$

which shows, specifically in this model, the ratio of viscous forces to capillary forces. In this equation, D, C_e, μ_l, and r_0 are a measure of gas-phase diffusivity, equilibrium concentration of the vapor which is a function of temperature, liquid viscosity, and the pore size, respectively. This capillary number was later used to characterize the porous medium; for a Ca < 0.1, the capillary forces are dominant and thus, liquid film flow is the main transport mechanism. Moreover, lower Ca means a higher extent of the liquid film.

As mentioned before, the formation of the liquid film is a work of capillary forces, while viscous forces as well as gravity act against it. A well-defined capillary number such as the one in equation (7) can be useful in terms of providing a quantitative measure for whether or not the liquid film formation occurs. Camassel et al. [50] also used a capillary number as well as a Bond number in order to assess the dominance of capillary forces over gravity and viscous forces, for square capillaries with different sizes (Figure 8). First, they calculated the pressure differences induced by gravity (ΔP_g), viscous forces (ΔP_{vis}), and capillary forces (P_c) as

$$\Delta P_g = \rho_l . g . L \tag{8}$$

$$\Delta P_{vis} \approx \frac{\lambda^2 . \beta . e . \mu . L}{\rho_l . {r_0}^2} \tag{9}$$

$$P_c = \frac{\lambda . \gamma}{r_0} \tag{10}$$

Here, ρ_l is the liquid viscosity, g is the gravitational acceleration, L is the corner length, $\lambda = 3.77$ a dimensionless shape factor when contact angle $\theta = 0$, β is the dimensionless resistance (which depends on corner geometry, surface shear viscosity, and contact angle, taken to be $\beta = 100$ for the square capillary), μ is the dynamic viscosity, r_0 is the pore size, and γ is the surface tension of the liquid. Also, e, the evaporation rate from the tip of the film (at the open end), can be estimated as [48], [50]

$$e = \rho_g . D . \frac{(c_i - c_\infty)}{\delta} \tag{11}$$

where ρ_g is the vapor density, D is the diffusion coefficient of the vapor, c_i and c_∞ are vapor mass fraction at the tip of the film and in the free stream, and δ is the length of the diffusive boundary layer.

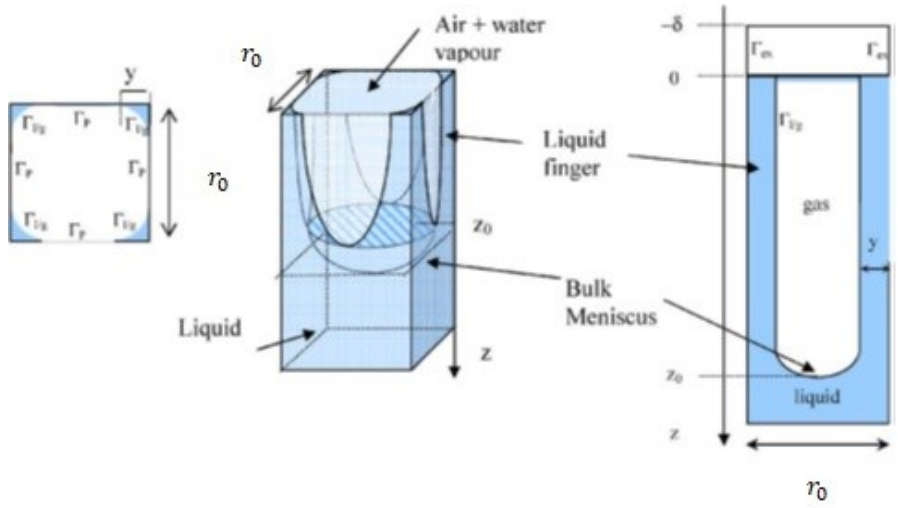

Figure 8- Convective evaporation in a square capillary initially saturated with a pure liquid followed by formation of the liquid films on the corners of the capillary [50]

The capillary (N_{vis}) and the Bond number (N_g) are then defined as the ratio of pressure difference due to viscous forces and gravity forces, respectively, to the pressure difference induced by capillary forces.

$$N_{vis} = \frac{\Delta P_{vis}}{P_c} = \frac{\lambda.\beta.e.\mu.L}{\rho_l.r_0.\gamma} \tag{12}$$

$$N_{vis} = \frac{\Delta P_g}{P_c} = \frac{r_0.\rho_l.g.L}{\lambda.\gamma} \tag{13}$$

Plotting these numbers against the tube size (r_0) illustrates that viscous and gravity effects can be neglected for tube sizes in the range of 10-100 µm, tube lengths L ≤ 0.1m, and evaporation velocities lower than 10^{-6} m/s. Evaporation velocity is defined as $\frac{e}{\rho}$, the ratio of evaporation rate to liquid density. An estimation of these numbers is presented for samples prepared in this work in the Discussion section.

While past studies on drying of a liquid in a porous media have been focused on water as the evaporating liquid [50]–[54], there has not been much work done on drying of porous materials wetted by organic solvents. Since the solids in our work are fully wetted by organic solvents, their drying mechanism is analogous to that of porous materials fully wetted by water. Here, instead of water, the organic solvent provides the hydraulic connectivity throughout the porous network via the formation of liquid films. Moreover, similar to the case of salt (a non-volatile solute) migration through capillary flow during evaporation of water [50], [52], [54], thick films of liquid solvent within the porous material play a major role in the migration and deposition of residual bitumen at the surface of the sample [44], [55]. This phenomenon, the deposition of a non-volatile solute on the surface of a porous material, is known as efflorescence effect and has been immensely studied for porous media wetted by water solutions [51], [54], [56].

1.5. Research Goal

In conclusion of previous studies, we learn that the major removal of cyclohexane occurs at the initial stage, where liquid film connectivity of cyclohexane exists. The drying rate at this stage is quite high, close to that of steady state evaporation of pure cyclohexane, which makes solvent removal fast and efficient even at ambient conditions.

The goal of this study is to investigate the role of varying composition of bitumen, water, and fines content on the initial evaporation rate of the cyclohexane from the gangue samples. We prepared synthetic “reconstituted gangue” samples with various bitumen, water, and fines contents and investigated the role of each component on the initial drying rate of the gangue. Furthermore, we will try to investigate the role of water by replacing it with 1 M NaCl solutions

(modifying solid surface potentials) as well as n-butanol (an organic liquid with volatility close to that of water). Eventually, we will offer an insight into the drying mechanism of solvent-extracted gangue of oil sands which can be used toward designing an effective drying technique on an industrial scale. With the results of this study, there will be a better understanding on how much solvent removal is affected by the original ore characteristics.

1.5.1. Drying of the Gangue

A typical drying curve, i.e., mass loss over time, of a porous medium such as a gangue sample, includes three stages: an initial stage with a fast, constant, and linear drying flux, a transition state where drying flux starts to drop, and a final stage with a constant, linear, and significantly lower drying flux compared to the initial stage.

It has been shown that at the initial stage, the wetting liquid film flow discussed in the previous section, is the major transport mechanism [46]. This liquid connectivity of the solvent within the porous medium accounts for the initial stage of fast, constant, and linear mass loss [46]. Therefore, in the beginning of the drying process, where there is enough liquid inside the porous material for liquid films to form, solvent is transferred by capillary forces through liquid films all the way to the evaporating surface of the sample, where it evaporates by a rate close to that of its free liquid evaporation. The drying rate remains practically constant, as long as the liquid films span across the entire pore network and provide hydraulic connectivity between the bulk liquid front and the surface of the sample [57].

The drying rate then starts to drop in the transition stage as the solvent film tips (the evaporation interface) recede below the surface of the sample, where the evaporated liquid must diffuse out of the tortuous path of the porous network.

Finally, the evaporation rate drops significantly (around one order of magnitude) compared to the initial drying rate. This is where liquid films of solvent are broken and thus, liquid solvent connectivity is lost. The solvent must evaporate in the pores which, requires a lot more energy and is substantially slower compared to evaporation at the surface.

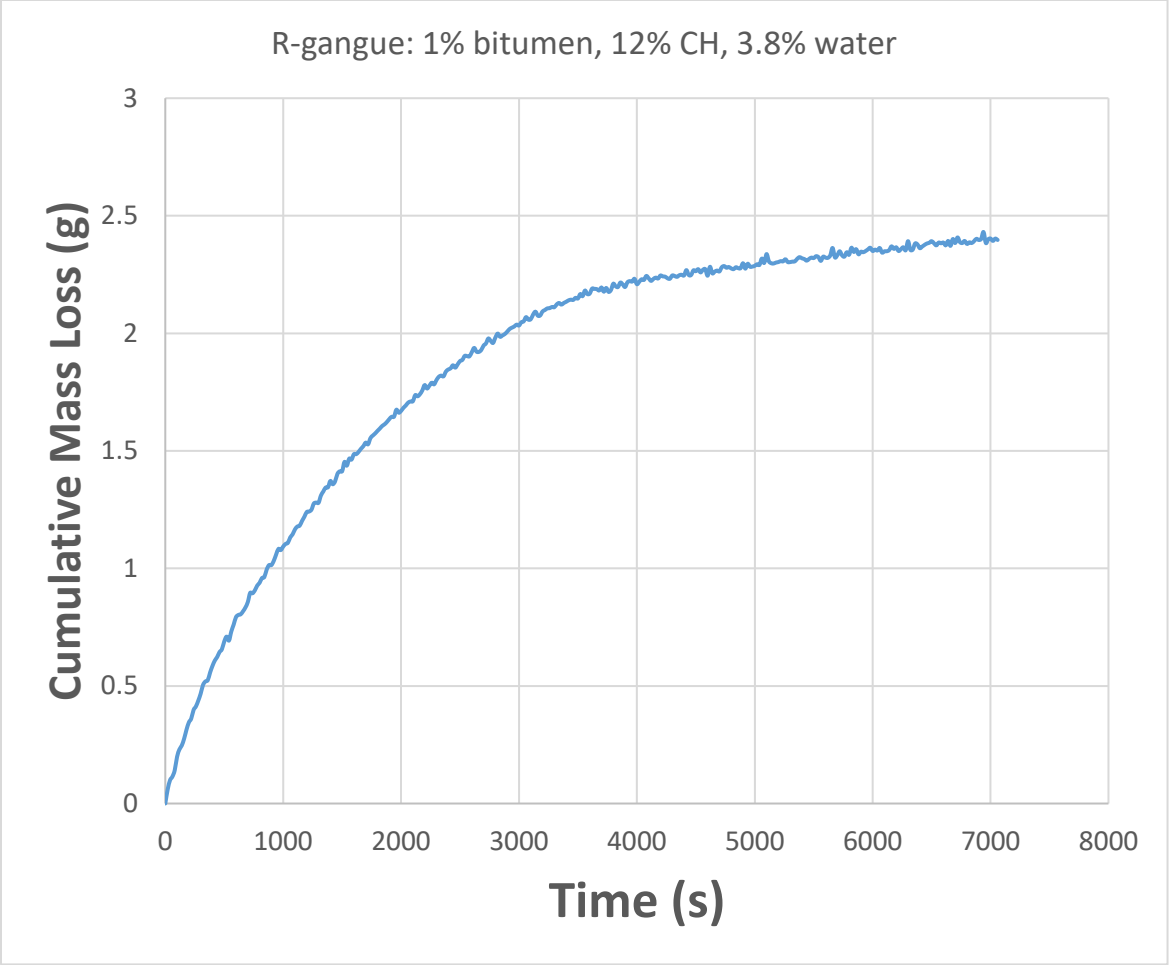

Figure 9- A typical drying curve of a gangue sample

This is due to the Kelvin effect which describes how the vapor pressure of a curved liquid surface in a pore is suppressed compared to that of a flat surface. The intensity of vapor pressure suppression is inversely correlated to the radius of curvature and described by Kelvin equation

$$\ln\left(\frac{P_0^K}{P_0}\right) = \frac{2V_m}{RT}\left(\frac{\gamma}{r}\right) \tag{14}$$

where P_0^K and P_0 are respectively the vapor pressure of the curved and the flat surface, and V_m, γ, R, T, and r are molar volume, surface tension, gas constant, temperature, and the radius of curvature, respectively. This equation stresses how evaporation becomes arduous in pores with

sizes of a few nanometers, given that the term $\frac{2V_m\,\gamma}{RT}$ is 1.05 nm for water ($V_m = 18\ cm^3$, $\gamma = 72\,\frac{mN}{m}$) and 2.14 nm for cyclohexane ($V_m = 108.17\ cm^3$, $\gamma = 24.6\,\frac{mN}{m}$)

There have been studies on the role of various operational and compositional parameters on the drying of the gangue. Renaud [55] studied the drying of gangue samples at different temperatures and pressures and also performed an energy efficiency analysis for each setting. The results suggested that elevating temperature and vacuum was energy efficient in the final slow stage of evaporation, but not so much in the initial fast drying stage. The two representative bar charts in Figure 10 demonstrate that removing the bulk of the solvent (in the initial stage of drying) is less accelerated by the increase in temperature compared to removing the trace amounts of solvents in the later stages. As discussed by Renaud, an extreme increase in temperature would decrease liquid films dominance in evaporation, and this explains why further increasing temperature was less beneficial at higher temperatures.

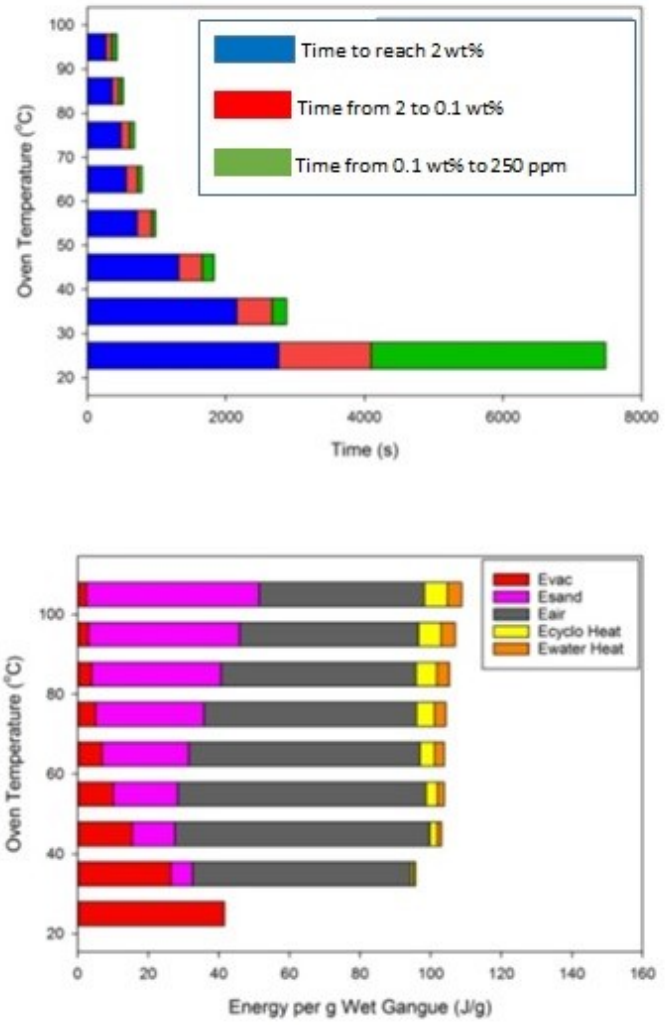

Figure 10 - Time and energy analysis of drying of a high grade cyclohexane-extracted gangue at 950 mbar and different temperatures [55]

Panda et al. [44] investigated the drying of gangue samples for 2 hours under ambient conditions, with different bed heights as well as different cyclohexane and bitumen contents. For samples with a bed height of 1 cm, they reported contents of residual cyclohexane above 260 ppm in samples with a bitumen content of 1.5 wt% or higher. These samples showed lower initial drying fluxes and resulted in high concentrations of residual cyclohexane (>260 ppm) in the gangue after

2 hours of drying. His results [47] suggest bed height to be a major parameter affecting the residual solvent concentration after 2 hours of drying. Decreasing bed height from 1 cm to only 0.6 cm, resulted in significant drops in residual cyclohexane concentrations, from above 200 ppm to lower than 60 ppm. Interestingly, there was no significant change in the initial drying fluxes in samples with different bed heights, which may be due to the presence of liquid films. Moreover, residual bitumen content had a significant effect on slowing down the initial drying stage and increasing the final residual cyclohexane. Panda [47] explained the effect of bitumen by how it affects "sorptivity," a quantity that expresses the ability of a porous material to absorb and transmit fluids via capillarity [56], [58]. Sorptivity is defined as the rate of a liquid's infiltration (i.e., the distance the liquid penetrates) into a porous material when plotted against the square root of time [59]

$$i = S.\sqrt{t} \tag{15}$$

And therefore, has a SI unit of $m.s^{-1/2}$ [58]. Sorptivity itself is defined as

$$S = S'.\sqrt{\frac{\gamma}{\mu}} \tag{16}$$

where γ, μ, and S' are respectively the surface tension, viscosity of the fluid, and intrinsic sorptivity of the material [58]. Intrinsic sorptivity is a quantity which includes the effect of all the parameters specific to the porous material characteristics, and therefore, is independent of liquid properties as well as temperature. It is interesting to note that it has a unit of $m^{1/2}$.

Panda explained how the presence of only 2.4 wt% bitumen can increase the viscosity of cyclohexane/bitumen solution by 50% and subsequently, drop the gangue's sorptivity by 20%.

Thus, the reduced initial drying rates were attributed to the decrease in sorptivity. It should be noted that in addition to decreasing sorptivity, bitumen also contributes significantly to solvent retention by absorption of cyclohexane [24].

Ejike [60] studied the drying of bitumen-free gangue samples with different amounts of fines. While increasing fines content generally resulted in higher residual cyclohexane contents, all samples showed a cyclohexane content below 40 ppm after 2 hours of drying, further highlighting the adverse effect of bitumen on solvent removal. Ejike reported that increasing the fines content reduced the duration of the initial drying stage but had no effect on the initial drying rate.

Role of water on drying of cyclohexane from the gangue has not been extensively studied. It has been shown that connate water in the ore helps bind the clay minerals together, preventing their transfer to bitumen product [16]. Nikakhtari et al. [42] added different amounts of water to samples of a rich grade oil sands ore prior to cyclohexane-based extraction and measured the drying rates of obtained gangue samples at different relative humidity and drying temperatures. While cyclohexane removal rates increased with the increase in temperature, its removal rate as well as its final residual content decreased as humidity was higher. Moreover, samples with water contents higher than 13 wt% led to significant drops in initial solvent drying rates and high residual solvent concentrations. Nikakhtari et al. [16] had previously concluded that the evaporation in the initial fast and final slow drying stages are solvent and water dominated, respectively. Anvari et al. [61] conducted a molecular dynamics simulation at 298.15 K and 1 atm to observe the behavior of water and cyclohexane confined in a model clay (kaolinite) nanopore (4-6 nm). Water bridges between the two basal surfaces were observed as water weight ranged between 6-30 wt% based on dry solids. However, when sodium chloride ions were added to the

aqueous phase at a concentration of 1 M, the bridge structure of water molecules was broken and the basal surfaces were fully wet by water. This observation was explained by the effect of ions on the solids' surface potentials.

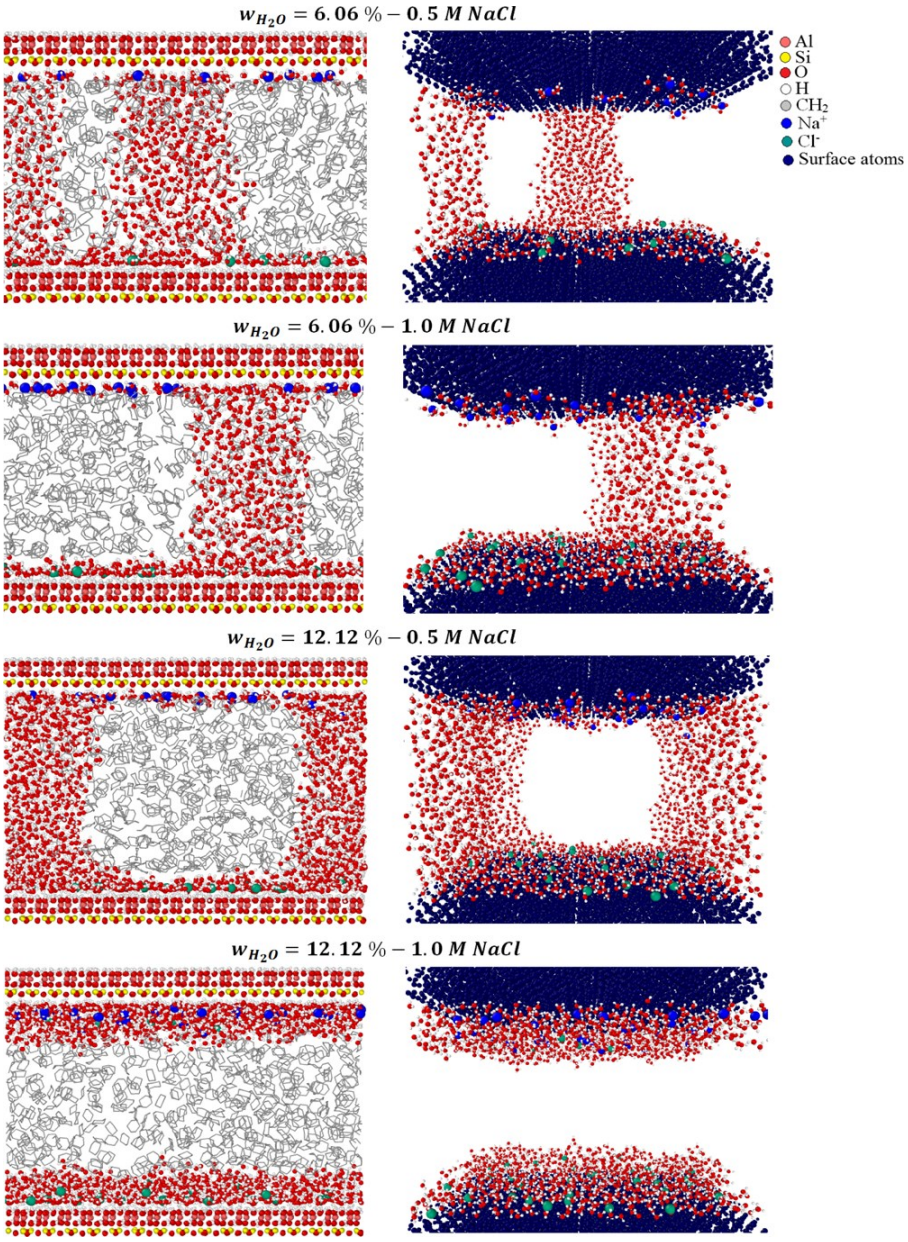

Figure 11 - Equilibrated state of the systems with the water content of 6.06 and 12.12% (based on dry solids) at different concentrations of NaCl. Notice how water bridges are broken at 1 M NaCl, fully detaching cyclohexane from solid's surface [61]

2.Methodology

2.1. Reconstituted Gangue

As mentioned before, the gangue after solvent extraction is a mixture of solids, residual bitumen, connate water, and residual solvent. It is a challenge to study the role of gangue's composition on its drying since the composition varies after each extraction [55]. To address this issue, we prepare artificially made "reconstituted" gangue samples with known compositions, based on a previously established method [47], [60]. In this method, bitumen, water, and the solvent are added, in controlled amounts, to solids obtained from oil sands extraction.

Panda [47] obtained and compared the drying behavior of solvent extracted gangues with reconstituted gangue samples to verify their similar drying trends. It should be noted that the aim for preparing and studying reconstituted gangue samples is not to obtain highly precise numbers which could be applied to real gangue samples. Instead, the goal here is to mimic the drying behavior of solvent extracted gangues in order to gain insight into the role of compositional parameters on the drying of the gangue. Therefore, the insignificant differences in the initial drying fluxes or the transition times in the two drying curves could be neglected.

The cyclohexane content of extracted gangue varies from 8-18% by weight with a mean and standard deviation of 11.8 ± 2.1% [55]. The residual bitumen content in the extracted gangue depends on bitumen extraction rate while water content is approximately the same as the original connate water content in the ore. In this study, Cyclohexane content in all the reconstituted gangue samples was fixed at 12.0 wt%, while water content ranged from 0.0-12.0

wt% and bitumen associated carbon (Bit.C) varied from 0.0-2.0 wt%, based on dry soxhlet solids weight.

Bitumen associated carbon (Bit.C) refers to the organic carbon whose source is bitumen. The sources of carbon in the samples prepared are bitumen and inorganic materials. Hence, subtracting the inorganic carbon wt% from the net measured C wt% in the sample gave us the Bit.C wt%. The inorganic C wt% in the samples was the C wt% of the Soxhlet solids used to prepare the reconstituted gangue. It should be stressed that a 0.0-2.0 wt% of Bit.C corresponds to 0.6-2.4 wt% bitumen, given 83.3 wt% carbon content of bitumen. This range of residual bitumen content in the gangue subsequently corresponds to an 84-96 % extraction recovery rate of bitumen, for a rich grade ore such as the one used in this study, having a bitumen content of ~11 wt%.

2.2. Materials Used

The sample of rich grade oil sands ore used was provided by Syncrude Canada Ltd. Certified ACS grade toluene and cyclohexane used for dean stark extraction of the oil sands ore as well as for reconstituted gangue preparation, were purchased from Fischer Scientific, USA. The obtained soxhlet solids from dean stark extraction were coated by Athabasca bitumen also provided by Syncrude. Cyclohexane (Certified ACS grade, Fischer Scientific, USA) and demineralized water were added to prepare the reconstituted gangue samples.

2.3. Dean Stark Extraction Analysis

Dean Stark analysis is a procedure of distillation extraction involving the vaporization of water in the ore sample by the boiling of extraction solvent followed by water condensation and collection in a calibrated trap (Schlumberger Oilfield Glossary) (Figure 12).

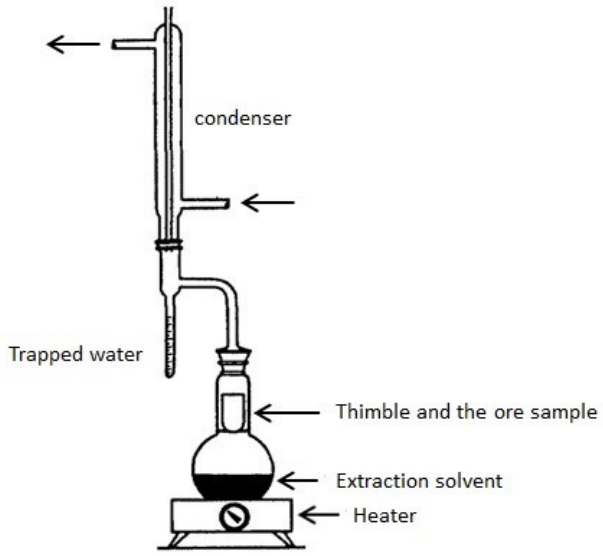

Figure 12- A schematic of dean stark extraction apparatus

Dean stark extraction was performed to determine bitumen, solids, and water content in the oil sands ore samples. Solvent is also condensed in the trap and allowed to overflow back over the sample placed in a thimble, to dissolve and extract bitumen. The extractions are stopped when the solvent dripping out of the thimble is visually clear. The thimble containing the extracted ore is dried to obtain mineral solids. The amount of collected water can be read from the calibrated trap and bitumen content can be determined by either mass balance (initial weight of the ore as well as weight of the extracted mineral solids and water are known) or removal of solvent from the solution obtained from the extraction. The mixture of fine and coarse solids obtained by

drying the collected solids in the thimble will henceforth be called “soxhlet solids.” For all the reconstituted samples in this study, solids particles >500 µm were separated from the rest of soxhlet solids in order to facilitate mixing and even distribution of bitumen on solids’ surface.

A total of 15 extractions were done to prepare the reconstituted gangue samples in this study. As described by Nikakhtari et al. [42], the extraction was performed with toluene for the first three times, and repeated with cyclohexane for the other 12 extractions. Cyclohexane was verified to have the same performance as toluene in terms of water and bitumen extraction. When using toluene, water is extracted from the ore due to azeotrope formation at 84.1 °C [62]. Water forms an azeotrope with cyclohexane too, at 69.8 °C [62]. In addition, equal amounts of solids and bitumen were obtained from toluene and cyclohexane extractions.

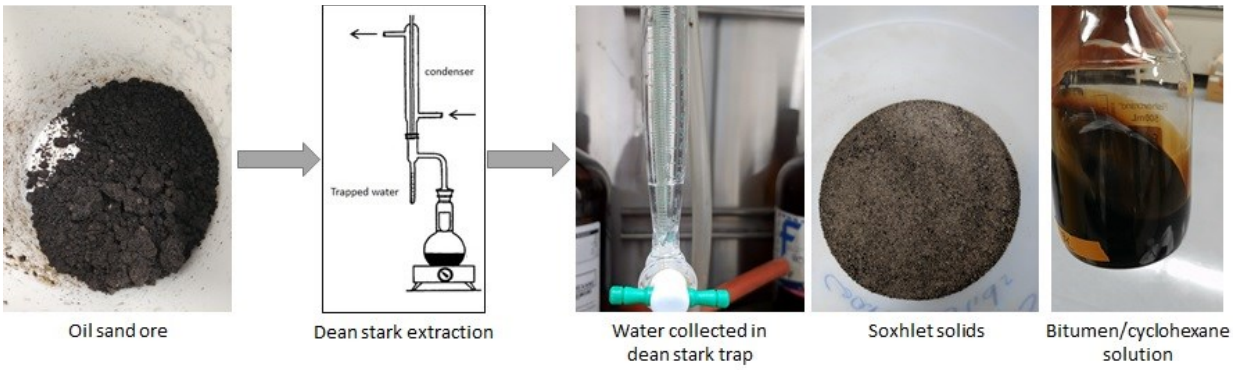

Figure 13- Separation of oil sands components (bitumen, water, and solids) using dean stark extraction

After conducting dean stark extraction on the oil sands ore sample for 24 hours, the solvent-wetted solids were allowed to dry, first under the fume hood for 1 hour, then in vacuum oven (at 80 °C and 30mbar) for 12 hours. The extracted bitumen/cyclohexane solution was centrifuged at 8 °C and 10000 RCF to verify that only trace amounts of fine solids (1.5 wt% of total fines) were transferred to the solution. Thus, the measured fines content in the extracted soxhlet solids was

assumed to be the same as the original fines content in the ore. The extraction thimble was weighed after the discharge of soxhlet solids in order to measure the weight of fine solids trapped in the pores of the thimble (the thimble is also weighed before dean stark extraction). The discharged dry (bitumen, water, and cyclohexane free) soxhlet solids were dry-sieved using a 45 µm aperture in order to isolate fine solids. Finally, fines content in the ore sample was calculated as the weight fraction of fine solids separated by dry-sieving plus the fines trapped in the pores of extraction thimble. It must be noted that the amount of fines transferred to the bitumen solution during dean stark extraction is also incorporated into fines content calculations, despite its negligibility.

$$Fines\ content\ (wt\%) = \frac{A + B + C}{total\ weight\ of\ solids\ collected\ after\ dean\ stark\ extractionn} \times 100 \qquad (17)$$

A – fine solids <45µm separated by sieving

B – fines trapped in the pores of extraction thimble

C – fines transferred to bitumen solution during extraction

Fine and coarse solids were later mixed again to desired proportions, before preparation of reconstituted gangue.

2.4. Preparation of Reconstituted Gangue

The protocol provided by Panda [47] with some modifications was utilized to prepare reconstituted gangue samples. Contrary to previous studies ([47], [60]), all of the composition measurements were done based on the weight of dry soxhlet solids. By considering solids as the basis, water and cyclohexane ratios could be compared for different samples because in this study, bitumen, water, and fines content varied.

It was assumed that the residual bitumen, water, and cyclohexane in the extracted gangue is distributed uniformly. This is a valid assumption considering that the steps involved in non-aqueous extraction of bitumen involves mixing and sieving [16] that should form an almost homogeneous product. The applied protocol to prepare reconstituted gangue is presented in Figure 14. All the steps shown in the flowsheet were carried out at room temperature (21 ± 1 °C) and ambient pressure conditions and will be explained in detail below.

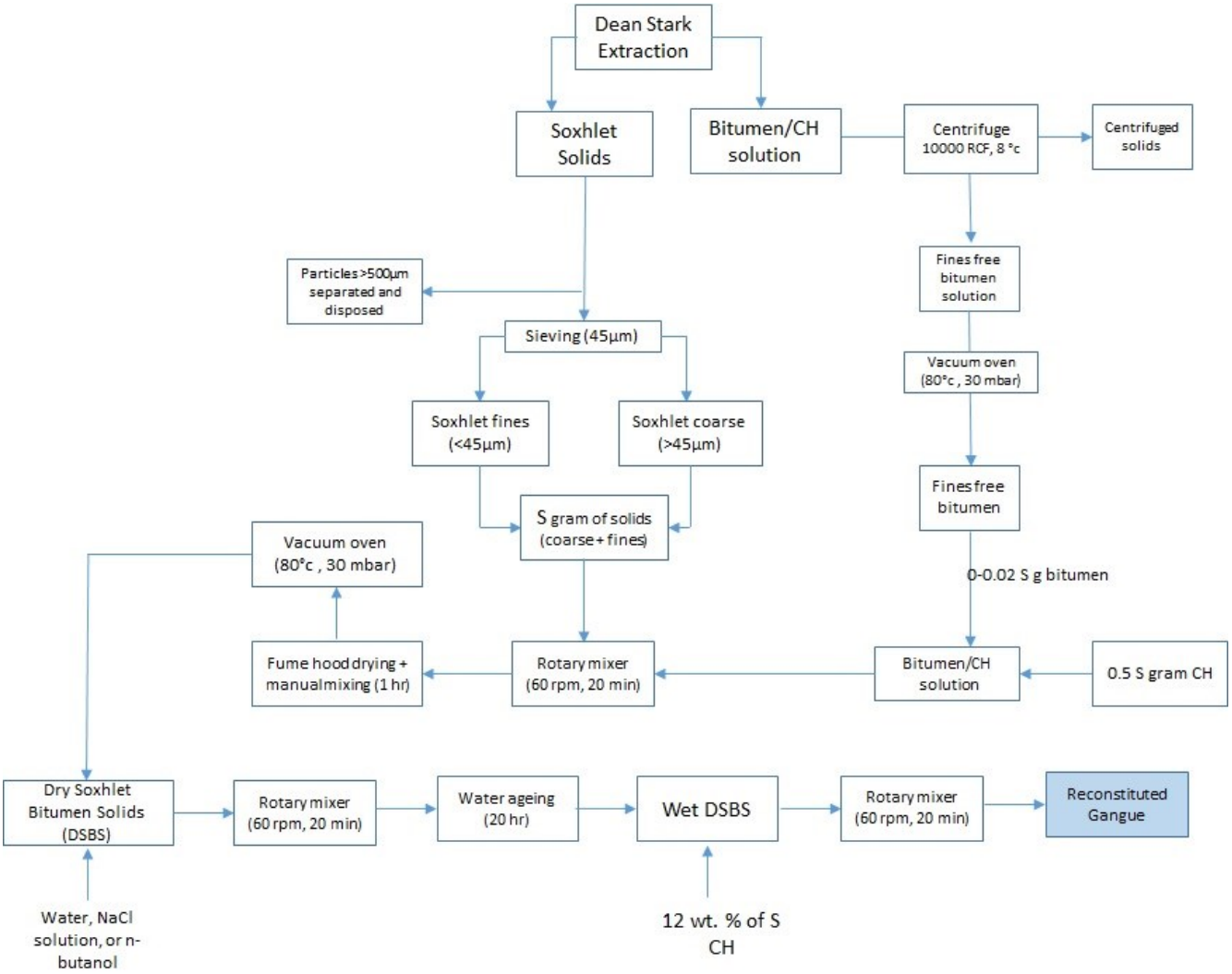

Figure 14 - Flowsheet for reconstituted gangue preparation (CH = cyclohexane)

About 100-200 g of Soxhlet solids was used for reconstituted gangue preparation per batch. An amount of cyclohexane (about half of soxhlet solids weight) was mixed with the required amount of bitumen to form the cyclohexane-bitumen solution. Based on the desired bitumen content, the amount of added bitumen was calculated as

$$Weight\ of\ bitumen\ added\ to\ solids = \frac{bitumen\ content}{100} \times weight\ of\ solids \quad (18)$$

Adding bitumen to the solids in a cyclohexane solution to make a slurry allows bitumen's uniform distribution in the gangue. Teflon bottles were used to store the (Soxhlet solids and cyclohexane-bitumen solution) slurry. The mixing was done using a rotary mixer at 60 rpm for 20 minutes. Next, the slurry was poured into a large glass beaker and was continuously mixed manually in the fume hood until the bulk of solvent evaporated. The manual mixing was essential for uniform distribution of bitumen. If the slurry is let dry with no manual mixing, due to efflorescence effect (discussed in Section 1.4.1), most of bitumen migrates to the open evaporating surface.

The product from the previous step, cyclohexane-wetted bitumen coated solids, was put in the vacuum oven (80 °C, 30 mbar) for 2-3 hours to ensure the complete removal of cyclohexane. The bitumen coated soxhlet solids produced from this step was called Dry Soxhlet Bitumen Solids or DSBS. Some of the DSBS was used for CHNS elemental analysis to verify bitumen content and its uniform coating of solids. For more on the CHNS analysis please refer to Section 2.6 and 3.3.

The water addition step begins with adding the required wt% of water to the DSBS put inside a Teflon bottle. Based on the desired water content, the amount of water added to a known amount of DSBS was calculated as

$$water\ added\ to\ DSBS = \frac{water\ content}{100} \times (1 - \frac{bitumen\ content}{100}) \times DSBS \quad (19)$$

The calculations were the same for samples with n-butanol instead of water. For samples with 1 M NaCl solutions instead of pure water, the amount of NaCl solution added was calculated so that the same water content would be obtained

$$1\ M\ NaCl\ solution\ added\ to\ DSBS = \frac{water\ wt\%\ in\ the\ solution}{100} \times water\ added\ to\ DSBS$$
$$water\ wt.\%\ in\ the\ solution = 1 - \frac{NaCl\ molar\ mass\ (\frac{g}{mol})}{density\ of\ 1M\ NaCl\ solution\ (\frac{g}{L})} \quad (20)$$

NaCl molar mass and density of 1M NaCl solution (at 20 °C) are 58.44 $\frac{g}{mol}$ and 1030 $\frac{g}{L}$, respectively.

The Teflon bottle was then sealed with parafilm and put on the rotary mixer at 60 rpm for 20 minutes. The wet DSBS in the sealed bottle was subsequently set aside for 20 hours to ensure water has enough time to enter into the pores of solids. This step, “water ageing” as called by Panda [47], is to replicate the proximity of water to solids’ surface and bitumen in the original ore.

Finally, a fixed amount of cyclohexane, 12.0 wt% for all the samples, was added to the wet water-aged DSBS. The Teflon bottle was immediately capped and sealed with parafilm and put on the rotary mixer at 60 rpm for 20 minutes. After this, the reconstituted gangue was ready for packing and drying.

2.5. Sample Packing & Drying Conditions

A gangue sample can be considered to be made up of porous soxhlet solids with bitumen, cyclohexane, and water in its pores. As will be discussed later, the density and porosity of the sample is a parameter at play in drying. Therefore, the prepared reconstituted gangue samples were evenly spread and packed into a glass petri-dish (OD 60 mm and height 15 mm, 50 mm ID, PYREX, CLS316060), to give a sample depth of 1 cm. This was to maintain a constant bulk density of 1.14 ± 0.17 g/cm^3 for dry soxhlet solids. The drying experiments were performed in a fume-hood. The sash height of the fume hood was kept constant to maintain a constant air flow of 95 feet per minute. The petri dish was next placed on the balance inside the fume hood at room temperature (20 °C) and ambient pressure (1 atm). The balance was connected to a computer which logged the weight of the sample every 20 seconds, using Mettler Toledo software.

2.6. CHNS Elemental Analysis

CHNS elemental analysis was used to determine carbon content of different samples. 3 sub samples (10-14 mg each) of each sample were carefully weighed in tin boats/capsules and placed inside the auto sampler unit of the elemental analyzer (Flash 2000 CHNS-O Analyzer, Thermo Scientific). Based on the sequence of loading, a sub sample was dropped into the quartz combustion reactor placed inside a furnace at a temperature of 900 °C. When the tin boat/capsule came in contact with oxygen in the immensely oxidizing environment of the reactor a strongly exothermic reaction was triggered. Temperature as high as approximately 1800 °C was reached causing sample combustion to occur instantly. The combustion products formed were transported across the reactor where the oxidation was completed. The Nitrogen oxides and

sulfur trioxides possibly formed were reduced to nitrogen and sulfur dioxide gases. The gas mixture from the combustion reactor comprising of CO_2, N_2, H_2O, $and\ SO_2$ were next separated in a chromatographic column. Finally, the eluted gases were passed onto a TCD (thermal conductivity detector). The TCD generates electric signals which was processed by the Eager Xperience software to provide us with the percentages of Carbon, Hydrogen, Nitrogen and sulfur present in the sub-sample. From dropping of a sub-sample into the reactor till obtaining the C, H, N and S percentages took approximately 12 min.

2.7. Contact Angle Measurements

Contact angle measurements were performed with placing a water droplet on the solid surface. The contact angle between water and the surface is a result of the equilibrium between the three phases and is quantitatively described by the well-known Young's equation[63]

$$\cos\theta_c = \frac{\gamma_{SG} - \gamma_{SL}}{\gamma_L} \tag{21}$$

Where γ_{SG}, γ_{SL}, and γ_L respectively represent solid-gas, solid-liquid, and liquid-gas interfacial tensions and θ_c represents the equilibrium contact angle.

Soxhlet sands have a porous and rough surface and thus, measuring contact angle by directly placing a water droplet on soxhlet sands' surface will not be accurate.

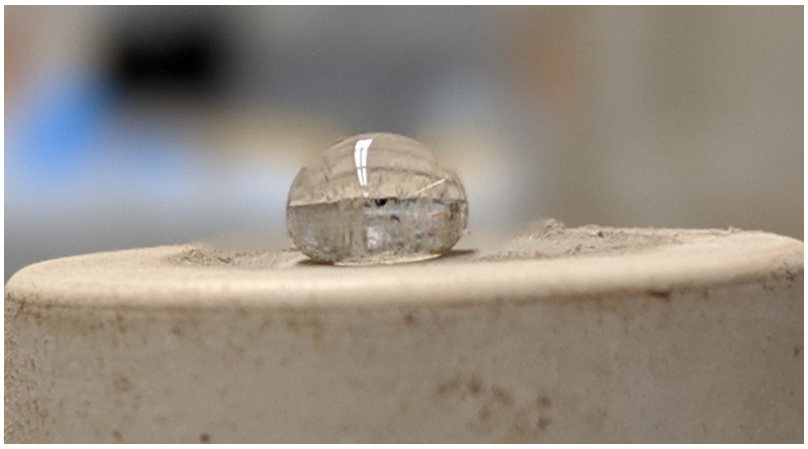

Figure 15- Placing a water droplet directly on compressed soxhlet solids' surface which is inaccurate due to surface roughness

Boric acid was used as a binding agent in order to obtain pellets of soxhlet solids with smooth homogeneous surfaces, as described by Huang [64]. First, 2g of boric acid was added to a 25.4 mm in diameter die as the bottom layer[65]. Next, 2g of manually mixed soxhlet solids and boric acid powder, with a weight mixing ratio of 1:1, was added on top of the bottom layer. The whole material was subsequently compressed in a manual hydraulic press (Enerpac JH-5) under 40 MPa pressure within 30 s.

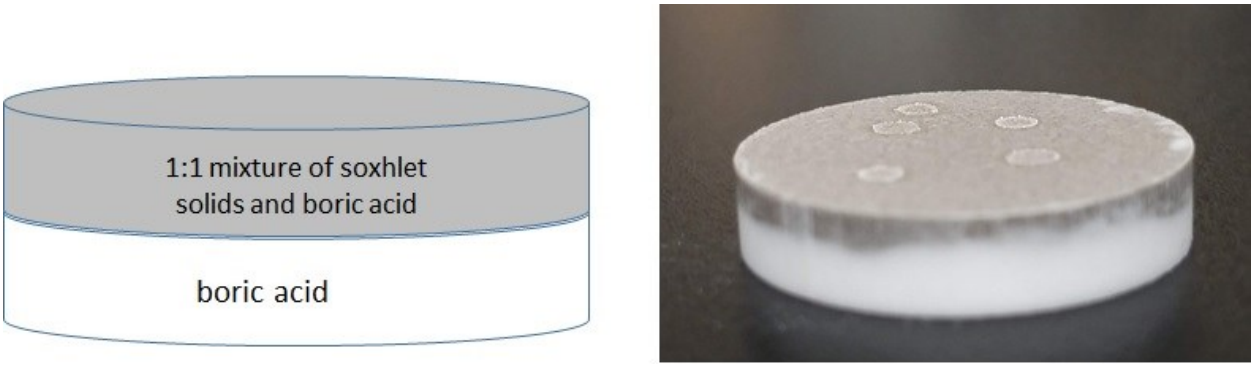

Figure 16- Schematic (left) and real (right) pictures of the pellets prepared for contact angle measurement

The resulted pellet has a surface of pure boric acid on one side, and a surface of 1:1 weight mixture of sample and boric acid on the other side (Figure 16). Knowing water contact angle with both

sides, we can determine soxhlet solids/water contact angle using Cassie-Baxter model [66] for a homogeneous composite surface

$$cos\theta_{CB} = f_s\, cos\theta_s + f_b\, cos\theta_b \quad (22)$$

Where θ_{CB} is the apparent contact angle on the composite surface (i.e. soxhlet solids and boric acid) θ_s and θ_b are the intrinsic contact angles of water with soxhlet solids and boric acid, respectively. f_s and f_b are respectively the area fractions of the soxhlet solids and boric acid on the surface and can be considered equivalent to their volume fraction, assuming homogenous distribution of the two components.

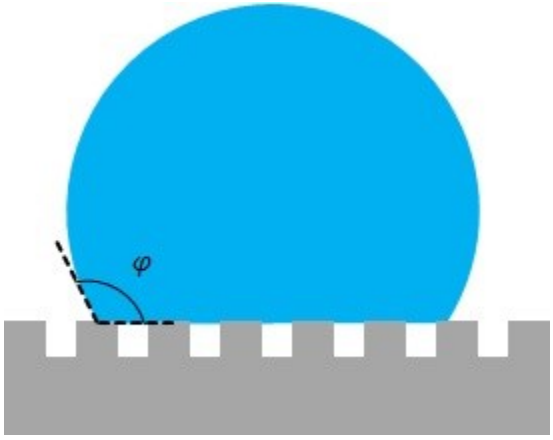

Figure 17 - Schematic representation of Cassie-Baxter model

A 5 µL water droplet, precisely controlled by a needle, was placed on the two surfaces of the pellets and pictures were captured. The water drop images were analyzed by a software based on the sessile drop technique. The measurements were repeated on different spots on the pellet and the mean value was reported.

2.8. Pycnometry Measurements

Pycnometry experiments with cyclohexane were carried out at room temperature to determine soxhlet solids' particle densities and porosities for different samples. Pycnometer's volume was first precisely measured by water and cyclohexane, separately. Solid particles density (ρ_p) was measured by obtaining the volume of a soxhlet solid sample with known mass. Next, soxhlet solids' bulk density (ρ_b) was measured using a graduated cylinder. As a result, porosity of the sample (ϕ) could be calculated [58]

$$\phi = \frac{\rho_p - \rho_b}{\rho_p} \tag{23}$$

3.Results

3.1. Ore Characterization

As mentioned in Section 2.3, the dean stark extraction was used to characterize the rich grade ore used in this work. The final results of the oil sands sample characterization are presented in Table 1. The mean and standard deviation values were calculated based on 15 extractions.

Table 1- Characterization of the oil sands sample used in this work

Bitumen [a]	Water [a]	Solids [a]	fine solids (>45µm)[b]
11.5 ± 0.8 wt%	3.1 ± 0.9 wt%	84.9 ± 0.6 wt%	6.8 ± 0.9 wt%

[a] *based on ore weight*
[b] *based on solids weight*

3.2. Porosity

Sample porosities were measured for three sets of DSBS samples with different fines contents. The results for the bulk density (ρ_{bulk}), particle density ($\rho_{particle}$), and porosity (ϕ) are presented in Table 2- Porosity results. The mean values and standard deviations are based on 3 measurements.

There are rigorous methods to obtain pore size distribution such as liquid (mercury or water) saturation or geometry image analysis [58]. However, obtaining a detailed distribution was out of this work's scope. Pore size distribution and particle size distribution are generally monotonic, i.e., wider particle size distribution means wider pore size distribution [67]. Therefore, in order to obtain a rough idea on pore size distribution, we can consider particle size distribution.

Table 2- Porosity results

Sample	ρ_{bulk}	$\rho_{particle}$	ϕ
Soxhlet solids after extraction (excluding >500 µm fraction)	1.42	2.76	0.48 ± 0.02
Soxhlet fines separated by sieving	0.60	1.78	0.66 ± 0.07
DSBS with 0% fines	1.23	2.36	0.48 ± 0.03
DSBS with 8% fines	1.37	2.29	0.40 ± 0.03
DSBS with 16% fines	1.50	2.34	0.36 ± 0.02

The dry bitumen-free soxhlet solids obtained after the extraction were passed through sieves with various mesh sizes. A mass fraction was obtained for each range of sizes, leading to a rough estimate of particle size distribution of solids. Particle size distributions for other samples were calculated and presented in Table 3Table 1.

Table 3 - Particle size distribution for different solid samples

Solids particle size (µm)	Soxhlet solids after dean stark extraction (wt%)	Soxhlet solids after removal of > 500 µm particles (wt%)	DSBS with 0.0 % fines (wt%)	DSBS with 8.0 % fines (wt%)	DSBS with 16.0 % fines (wt%)
lower than 45	6.80	7.33	0.00	8.00	16.00
45 - 150	25.10	27.05	29.19	26.85	24.52
150 - 212	50.10	53.99	58.26	53.60	48.93
212 - 500	10.80	11.64	12.56	11.55	10.55
higher than 500	7.20	0.00	0.00	0.00	0.00

We refer to solids with sizes smaller than 45 µm as “fines” in this study but we did not obtain fine solids particle distribution. Nikakhtrari et al. [20] reported that the fines fraction of soxhlet solids obtained from Athabasca oil sands is mainly consisted of clay particles (<2 µm). Moreover, Ejike [60] obtained a particle size distribution for two Athabasca ores (rich and poor grades) and reported that 50% of fines (D50) have a particle size <9 µm (Table 4). As a result, it can be deduced that increasing fines content leads to a lower porosity and wider pore size distribution.

Table 4 - From [59]: D10, D50, and D90 of a rich and a poor grade ore

Sample	Constituent Solid	D10 (µm)	D50 (µm)	D90 (µm)
Rich-grade	Fines (<45 µm)	1.6 ± 0.1	9.0 ± 0.9	41.3 ± 3.4
	Coarse (<45 µm and > 300 µm)	122 ± 4	190 ± 1	292 ± 4
Low-grade	Fines (<45 µm)	1.6 ± 0.1	8.9 ± 1.2	38.5 ± 2.4
	Coarse (<45 µm and > 300 µm)	75 ± 5	155 ± 5	277 ± 5

3.3. CHNS results

We used CHNS analysis on multiple samples. It helped us verify bitumen uniform distribution in the DSBS. Also, CHNS analysis was used to determine the carbon content of soxhlet fines, which was much higher compared to that of soxhlet solids (coarse + fine solids). The results of CHNS analysis are presented in Table 5.

Table 5- CHNS analysis results of carbon content measurements

sample	Carbon wt%	Bitumen wt%
Bitumen	C_b = 83.3 ± 0.04	100
Soxhlet coarse solids	C_c = 0.11 ± 0.09	0
Soxhlet fines	C_{fines} = 4.46 ± 0.02	0
DSBS (1.0 wt% bitumen) (no fine separation, fines content = 6.8 wt%)	C_{dsbs} = 1.32 ± 0.05	1.11
DSBS _f0 (1.0 wt% bitumen) (fines content = 0.0 wt%)	C_{dsbs_0} = 1.11 ± 0.08	1.20
DSBS _f8 (1.0 wt% bitumen) (fines content = 8.0 wt%)	C_{dsbs_8} = 1.81 ± 0.08	1.62
DSBS _f16 (1.0 wt% bitumen) (fines content = 16.0 wt%)	C_{dsbs_16} = 2.07 ± 0.09	1.53

The bitumen content of any component in this table is calculated as

$$Bitumen\ wt\%\ in\ A = \frac{C_A - C_s}{C_b - C_s} \times 100 \quad (24)$$

Carbon content of soxhlet solids (C_s) was calculated based on carbon content of the coarse and fine solids and their corresponding weight fractions. It should be noted that fines have a substantially higher carbon content (4.46 ± 0.02 wt%) compared to soxhlet solids, i.e., coarse and fines solids (0.37 ± 0.03 wt%). This is due to the precipitation of heavier fractions in bitumen, such as asphaltenes, on fines solids' surface [68]. These heavier fractions are not cyclohexane soluble. Therefore, they were not taken into account for DSBS preparation and thus, the calculations for

the added amount of bitumen to soxhlet solids were made based on the weight of dry soxhlet solids.

3.4. Contact Angle Results

According to the discussion in the previous section, same wt% of bitumen was added to the samples with different fines content despite higher carbon content of the samples with more fines. Therefore, it was assumed that bitumen/cyclohexane solution in all samples had the same viscosity due to the same amount of "soluble" bitumen. However, it was expected that the substantially higher carbon content of the samples with higher fines content would change their wettability by and affinity to cyclohexane. Contact angle measurements were performed to verify if there was any change in samples' affinity to solvent, i.e. hydrophobicity.

The effect of a higher carbon content in samples with higher amounts of fines could be observed in water contact angle measurements. The results are presented in Figure 18 and

Table 6. To calculate the contact angle of DSBS sample based on (22) , we considered the area fraction of each component to be equal to their volume fractions. Therefore, area fractions of DSBS and boric acid were 0.38 and 0.62, based on a 0.5 mass fraction and densities of 1.44 and 2.3 $\frac{g}{cm^3}$, respectively. Also, water contact angle of boric acid was measured on the other side of pellets to be 54.1°.

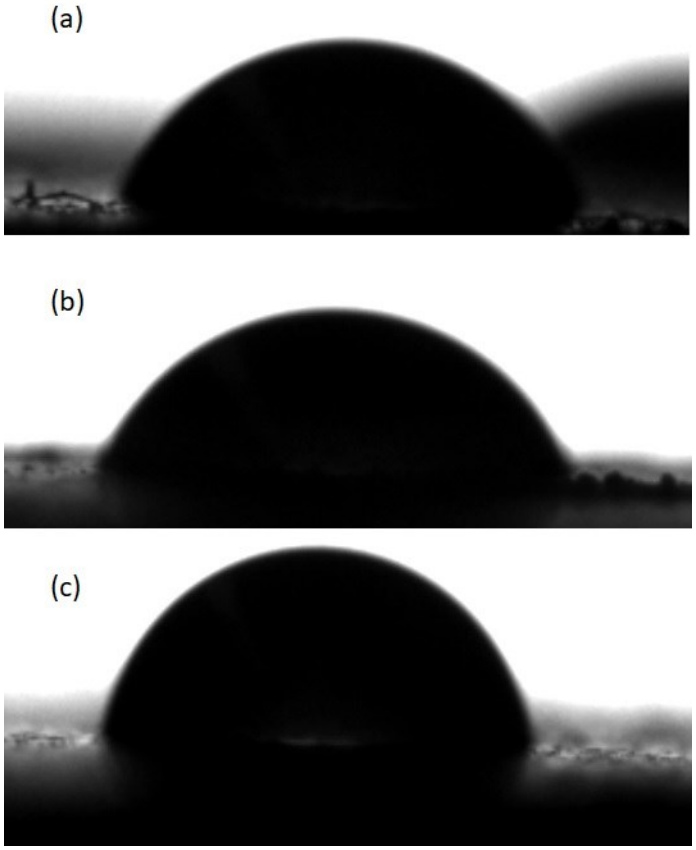

Figure 18- Water contact angle measurements on pellets made from boric acid and DSBS with different fines content

Table 6- Contact angle measurement results for DSBS samples with different fines content

sample	Apparent contact angle(°)	DSBS-water contact angle (°)
DSBS with 0% fines	56.3	59.70
DSBS with 10% fines	58.1	64.16
DSBS with 20% fines	69.3	91.06

3.5. Compositions of Reconstituted Gangue Samples

Compositions of the drying reconstituted gangue samples prepared in this work are shown as follows:

- Bitumen variation: 3 sets of samples with 0.0, 1.0, and 2.0 wt% bitumen. All had 3.88 wt% water, 12 wt% cyclohexane, and 6.8 wt% fines (the original ore's fine content)
- Water variation: All had 1.0 wt% water, 12 wt% cyclohexane, and 6.8 wt% fines (the original ore's fine content)
    - 4 sets of samples with 0.0, 3.88, 6.0, and 12.0 wt% water
    - 3 sets of samples containing 1 M NaCl solutions with 3.88, 6.0, and 12.0 wt% water
    - 4 sets of samples with 0.0, 3.88, 6.0, 12.0, and 25.0 wt% n-butanol
- Fines variation: 3 sets of samples with 0.0, 8.0, and 16.0 wt% fines. All had 1.0 wt% bitumen, 3.88 wt% water, and 12 wt% cyclohexane

3.6. Initial Drying Flux Determination

The reconstituted gangue sample's weight was logged every 20 seconds while the sample was dried in the fume hood. The cumulative mass loss was plotted against time as shown in Figure 9-A typical drying curve of a gangue sample. A linear regression was fit on the first 10 minutes of the cumulative mass loss vs time plot. As proposed by Panda [47], the slope obtained from the regression was used to define the initial drying flux

$$Initial\ drying\ flux = \frac{The\ slope\ of\ the\ linear\ regression\ fit\ in\ the\ first\ 10\ minutes}{Petri\ dish\ area\ (= 19.64\ cm^2)} \quad (25)$$

We believe a faster initial stage of drying can play an important role in faster and more efficient removal of cyclohexane. At ambient conditions, the initial drying stage is substantially fast and cyclohexane-dominated due to liquid film flow [16], [46]. More than 80% of the solvent evaporates at this stage with a rate close to that of steady state pure liquid evaporation. Therefore, there is no need for any energy input at this stage. This has also been shown before that increasing temperature and applying vacuum is much less effective in the initial stage than the final stage (Figure 10) [55].

However, the removal of cyclohexane in the final stage is substantially slow and its efficient removal requires more energy input, i.e., applying heat and vacuum. The evaporation of cyclohexane in the final stage, when liquid film connectivity is lost, requires higher amounts of energy due to Kelvin effects in the pores (equation (14). In addition to slow evaporation, the residual cyclohexane needs to diffuse out of the tortuous path of pores which is also a very slow process.

Panda [47] measured the residual solvent content in the reconstituted gangue samples after 2 hours of drying at ambient conditions. The results of his work (Table 7) suggest that bed height and the initial drying rate are the major parameters controlling the final residual solvent concentration. It is evident that transition time has an inverse correlation with the initial drying flux. Moreover, for the samples with 12 wt% cyclohexane and a 1 cm bed height, residual cyclohexane concentrations higher than 260 ppm (acceptable minimum) were obtained when the initial drying flux was below $30 \times 10^{-4}\, g/min.cm^2$. Therefore, in this work, we focused on the effect of compositional parameters on the initial drying flux as the major parameter controlling cyclohexane removal at ambient conditions.

Table 7 - A summary of results from [47]*: bed height and initial drying flux are the main parameters affecting the final residual cyclohexane content*

		Bed height = 0.6 cm				Bed height = 1 cm				
Bit.C wt%		0	1	1.5	2	0	0.5	1	1.5	2
8 wt% cyclohexane	**Initial drying flux × $10^{-4}\ g/min.cm^2$**	2.1	2	1.8	1.8	2.6	2.1	2	1.7	1.6
	Transition time (min)	35	35	45	40	55	70	80	90	90
	Residual CH (ppm)	<10	<10	10-50	<20	-	<100	<200	<200	<200
12 wt% cyclohexane	**Initial drying flux × $10^{-4}\ g/min.cm^2$**	3.6	3	2.5	2.3	3.6	3.6	3.5	2.5	2.3
	Transition time (min)	30	35	45	50	55	70	80	90	100
	Residual CH (ppm)	<20	<60	<60	<60	-	<200	<200	180-260	200-600

3.7. Representation of Drying Data

One batch of DSBS was used for a set of samples with one varying component. In addition, the drying experiments for samples with one varying component were performed consequently. For instance, to obtain the drying curves of samples with different water contents, one batch of DSBS was used to prepare samples with 0.0, 3.88, 6.0, and 12.0 wt% water contents, and the drying experiments were performed in one day. This was repeated with another batch of DSBS on another day.

The cumulative mass loss vs time was plotted for each reconstituted gangue sample. The drying experiments were conducted in triplicates. The reported initial drying flux and the upper and

lower limits are the mean and standard deviation values of three curves. The curves shown in the following sections are representative plots of each sample, displaying the general drying trend for different compositions.

As mentioned earlier, the initial and final drying fluxes are dominated by cyclohexane and water evaporation, respectively. Evidently, the evaporation rate of pure cyclohexane is the upper limit of the initial drying flux. For comparison, the evaporation curves of cyclohexane and water were also plotted with all the drying curves. These curves were obtained by plotting the mass loss of the pure liquid vs time, under the same experimental conditions.

3.8. Bitumen Content

Reconstituted gangue samples were prepared with 0.0, 1.0, and 2.0 wt% Bit.C (corresponding to 0.0, 1.2, 2.4 wt% bitumen, respectively). All samples contained a fixed amount of 12 wt% cyclohexane and 3.88 wt% water, based on dry soxhlet solids. 3.88 wt% of water based on dry soxhlet solids translates to 3.7 wt% water based on the oil sands ore, mimicking the connate water content in the ore. The drying curves and the initial drying fluxes are presented in Figure 19, along with the evaporation curves of pure liquid cyclohexane and water.

The detrimental role of residual bitumen content on the initial drying flux of the reconstituted gangue samples can be clearly observed. Increasing the Bit.C content from 0.0 wt% to 1.0 and 2.0 wt% results in 40% and 50% reductions on the initial drying fluxes, respectively, indicating the clear adverse effect of bitumen content on the drying of gangue samples. This is in agreement with the previous study by Panda et al. [44]. They observed the same trend in drying of reconstituted gangue samples with different bitumen concentrations.

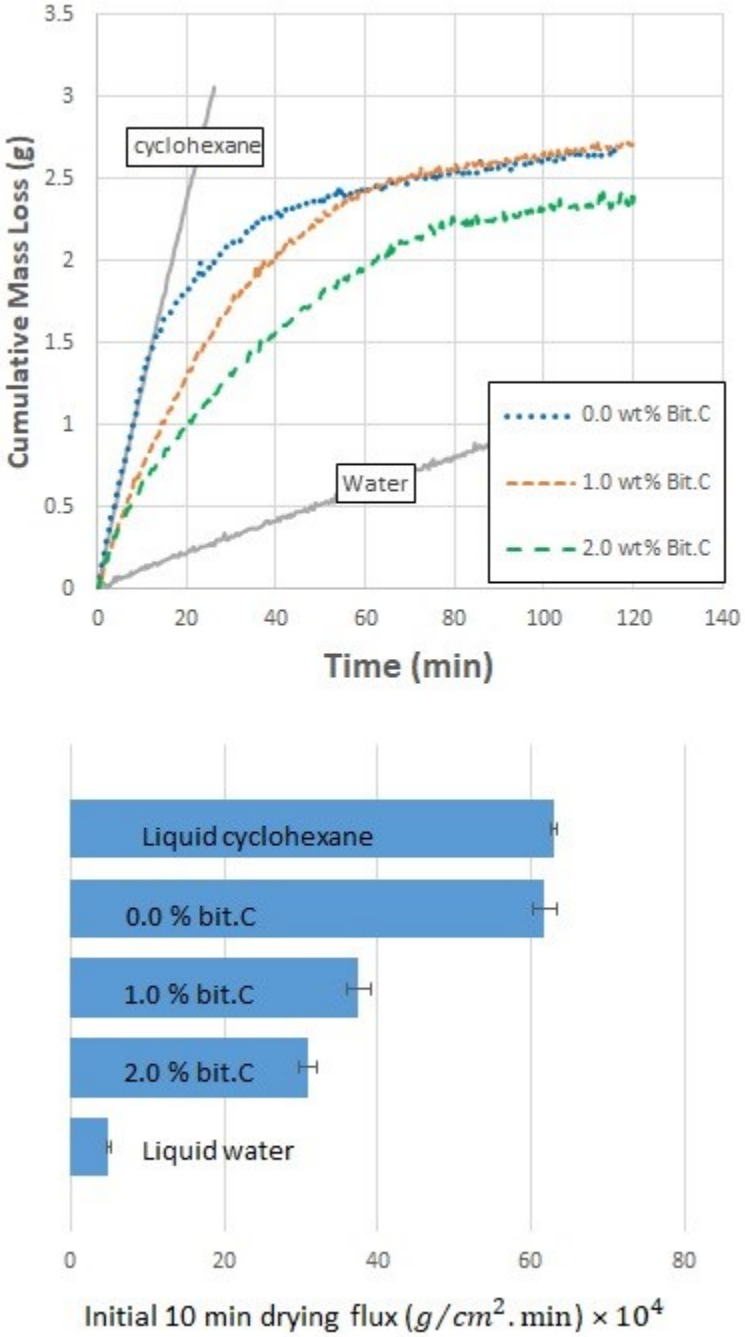

Figure 19 – (top) Drying curves of reconstituted gangue samples with 12 wt% cyclohexane, 3.88 wt% water, and 0.0, 1.0, and 2.0 wt% Bit.C (bottom) the initial drying flux obtained from the drying curves

3.9. Water Variation

Samples with 0.0, 3.88, 6.0, and 12.0 wt% water were prepared. All samples contained a fixed amount of 12 wt% cyclohexane and 1.0 wt% Bit.C, based on dry soxhlet solids. The drying curves and the initial drying fluxes are presented in Figure 20, along with the evaporation curves of pure liquid cyclohexane and water. In addition, the drying of a sample with 25 wt% water (to achieve full saturation of pores) was also performed. The initial drying flux was significantly low (even lower than pure water evaporation rate) and thus, the results were not presented here.

The initial drying flux drops more than 50% for samples with water contents of 12 wt% compared to the sample with 6 wt% water. This was in agreement with another study on the impact of water on drying rates [42]. As lowering water content from 12 wt% to 6 wt% increased the drying rate, further lowering water content was expected to enhance the drying performance. However, the sample with 3.88 wt% water showed almost the same initial drying rate compared to the sample with 6.0 wt% water. In addition, a lower drying rate was interestingly observed for the sample with no water compared to samples with 3.88 and 6.0 wt% water.

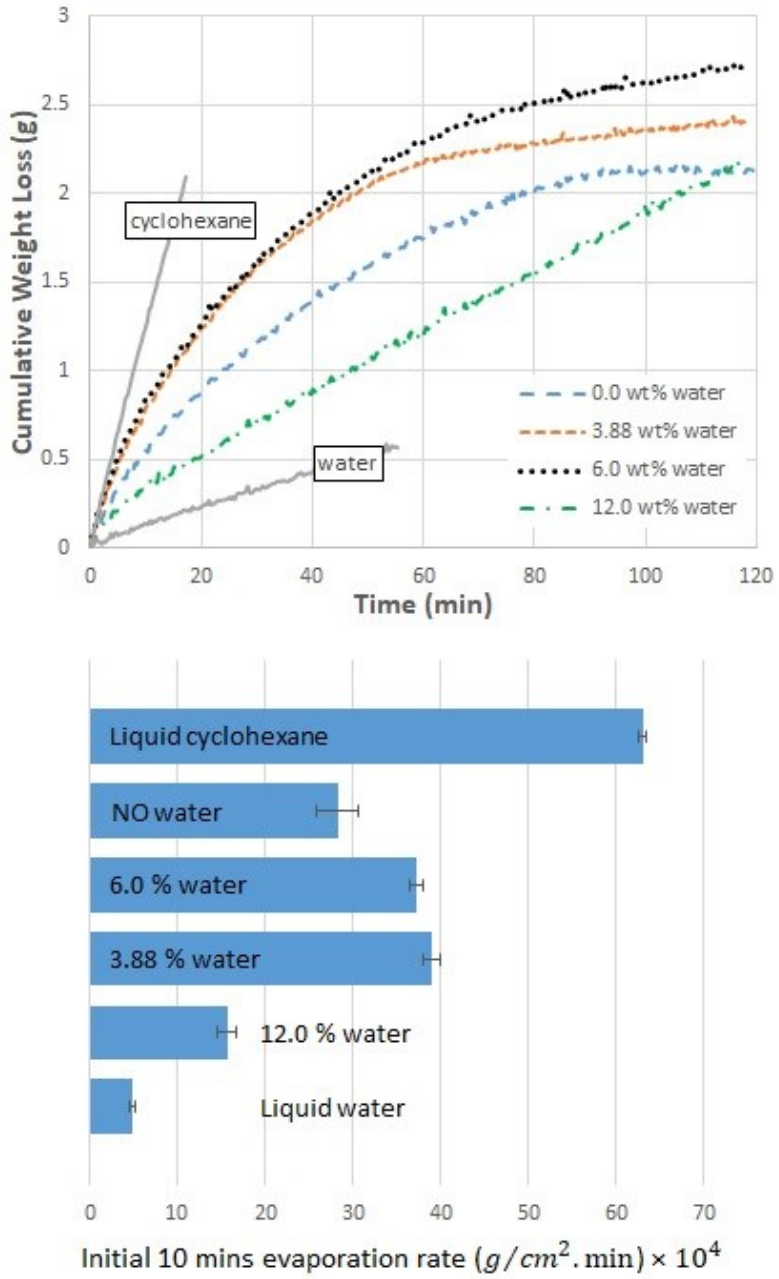

Figure 20- (top) Drying curves of reconstituted gangue samples with 12 wt% cyclohexane, 1.0 wt% Bit.C, and 0.0, 3.88, 6.0, and 12.0 wt% water (bottom) the initial drying flux obtained from the drying curves

Another interesting observation was the minor migration of bitumen to the surface of the sample with no water. Bitumen migration to the top of the gangue sample along with cyclohexane

evaporation is an example of efflorescence formation [54] which was previously observed and reported [44], [55]. It happens at the initial stage of drying where due to the capillary action, bitumen is moved to the surface through cyclohexane liquid film and deposited after cyclohexane evaporation. After 2 hours of drying, the dark discreet deposited layer of bitumen can be seen at the top layer of the sample with 3.88 wt% water (Figure 21a). Bitumen deposition in the sample with 3.88 wt% water is so effective that the top layer of the sample can be peeled off as a separate layer (Figure 21b). Yet, bitumen is merely deposited in the sample with no water, where no distinctive peel able dark layer of bitumen is obtained (Figure 21c).

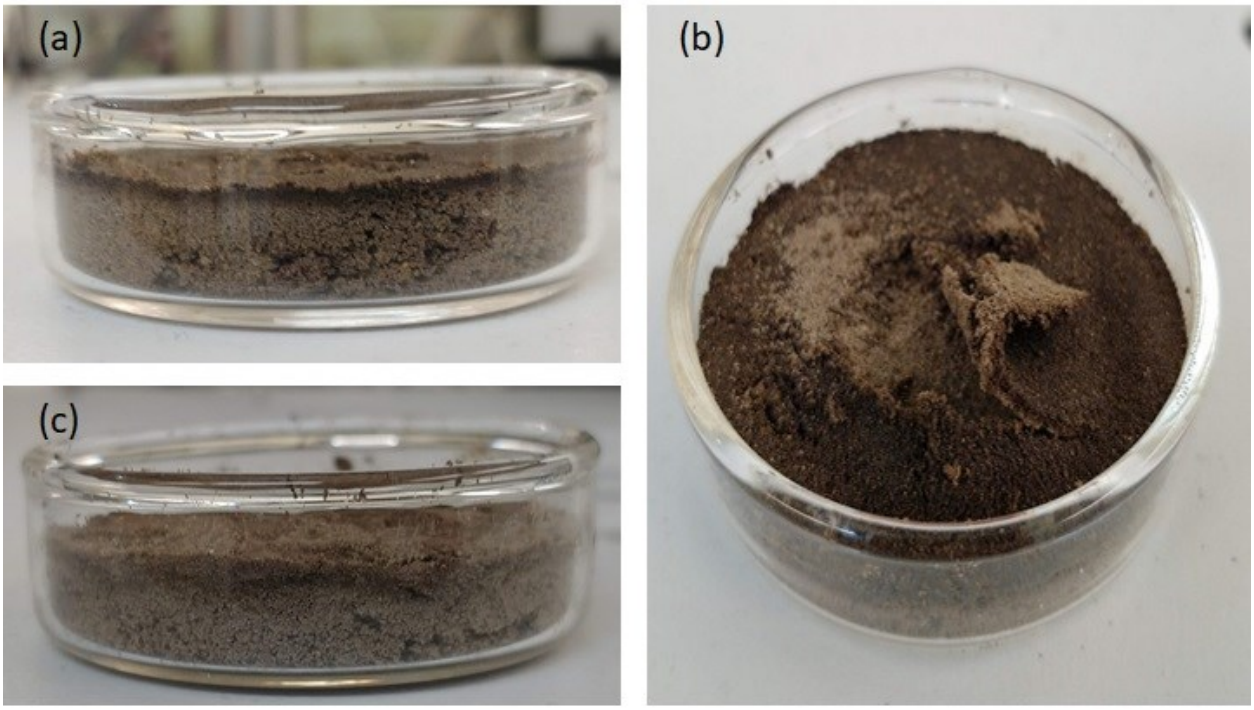

Figure 21 – (a) formation of thick dark layer of bitumen due to bitumen migration and deposition in the top layer of samples with 3-6 wt% water, after 2 hours of drying; (b) top view of the sample in a: bitumen deposition is quite significant that the bitumen deposited top layer can be easily peeled off; (c) weak deposition of bitumen in samples containing no water. No peel able layer formed

3.9.1. Replacing Water with n-butanol, an Organic Liquid

To compare and further investigate the effect of water on the initial drying rate of cyclohexane, we prepared samples in which water was replaced by n-butanol. N-butanol is an organic liquid, miscible with cyclohexane, and has similar-to-water low vapor pressure and high boiling point (Table 8).

Table 8 - Vapor pressure and boiling point of cyclohexane, n-butanol, and water

	Vapor pressure (kPa at 25 °C)	Boiling Point (°C)
Cyclohexane	13.0	80.7
n-butanol	0.92	117.7
water	3.16	100

The procedure and calculations of adding n-butanol was the same as water. Figure 22 - (top) Drying curves of reconstituted gangue samples with 12 wt% cyclohexane, 1.0 wt% Bit.C, and 0.0, 3.88, 6.0, and 12.0 wt% n-butanol (bottom) the initial drying flux obtained from the drying curves illustrates the drying curves of samples with 3.88, 6.0, 12.0, and 25.0 wt% n-butanol as well as pure liquid cyclohexane, pure liquid water, and the gangue sample with 3.88 wt% water for comparison.

The drying curve of a 5 g sample of 1:1 wt liquid mixture of n-butanol/cyclohexane (no solids) is also shown in Figure 22. In drying of the liquid mixture of n-butanol/cyclohexane, cyclohexane, as the volatile component, almost fully evaporates first. Interestingly however, cyclohexane evaporation is completely different in the gangue, with the presence of solids. All the

reconstituted gangue samples with different amounts of n-butanol, show significantly low and similar drying rates.

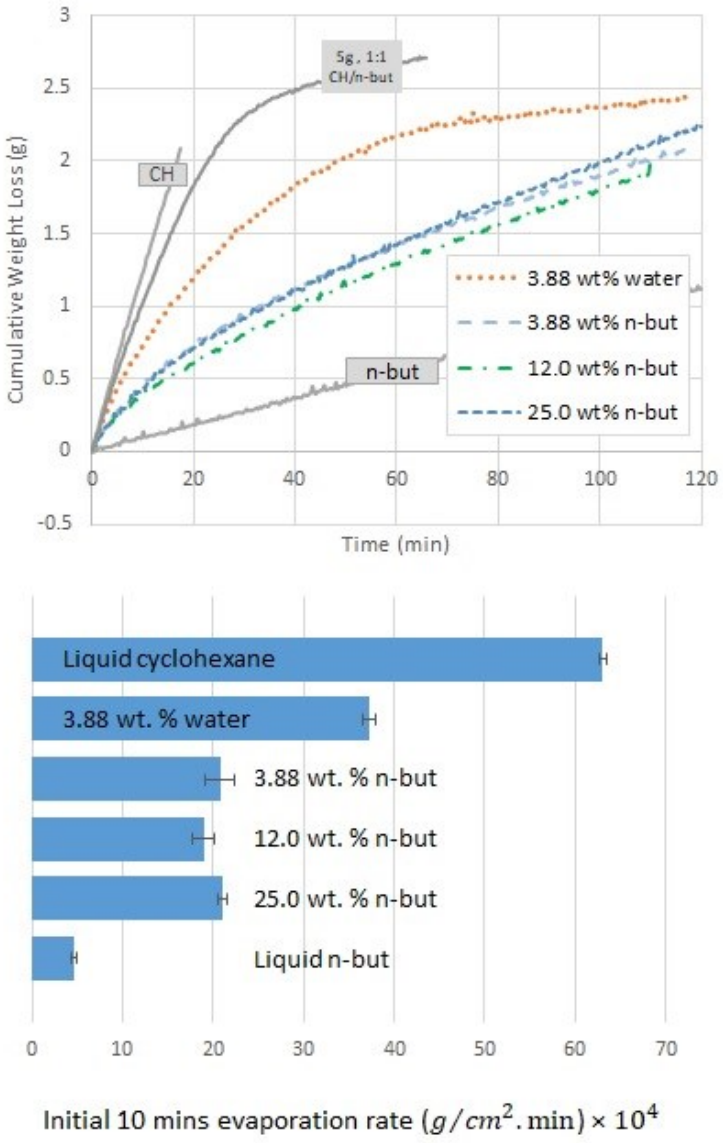

Figure 22 - (top) Drying curves of reconstituted gangue samples with 12 wt% cyclohexane, 1.0 wt% Bit.C, and 0.0, 3.88, 6.0, and 12.0 wt% n-butanol (bottom) the initial drying flux obtained from the drying curves

3.9.2. Replacing Water with NaCl Solution

Samples with 1 M NaCl solution instead of water were prepared. The samples contained 0.0, 3.88, 6.0, and 12.0 wt% water. All samples contained a fixed amount of 12 wt% cyclohexane and 1.0 wt% Bit.C, based on dry soxhlet solids. The drying curves and the initial drying fluxes are presented in Figure 23. As can be seen, there is almost no difference between the samples with NaCl solution and water.

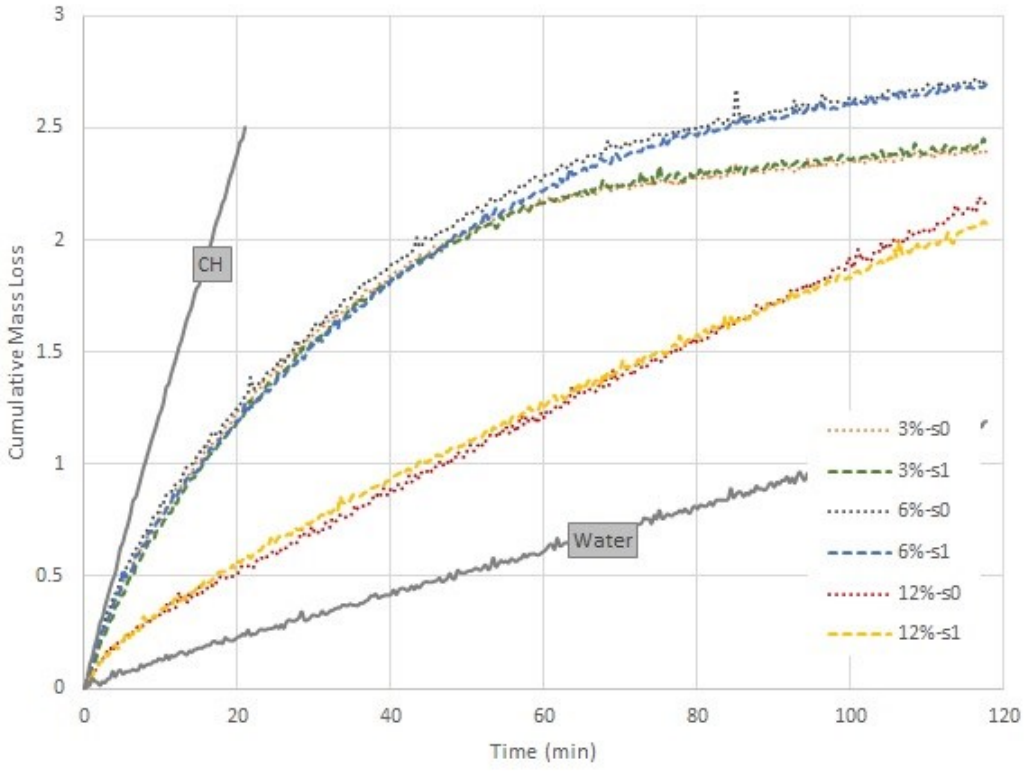

Figure 23 - Drying curves of reconstituted gangue samples with water and 1 M NaCl solution, containing 12 wt% cyclohexane, 1.0 wt% Bit.C, and 0.0, 3.88, 6.0, and 12.0 wt% water

3.10. Fines Variation

Samples with 0.0, 8.0, 16.0 wt% fines were prepared. All samples contained a fixed amount of 12 wt% cyclohexane, 3.88 wt% water, and 1.0 wt% Bit.C, based on dry soxhlet solids. Fines content was controlled by mixing coarse and fine solids in desired proportions before preparing DSBS.

The drying curves and the initial drying fluxes are presented in Figure 24, along with the evaporation curves of pure liquid cyclohexane and water. Figure 24 illustrates that there is no significant difference in drying of samples with different fines compositions.

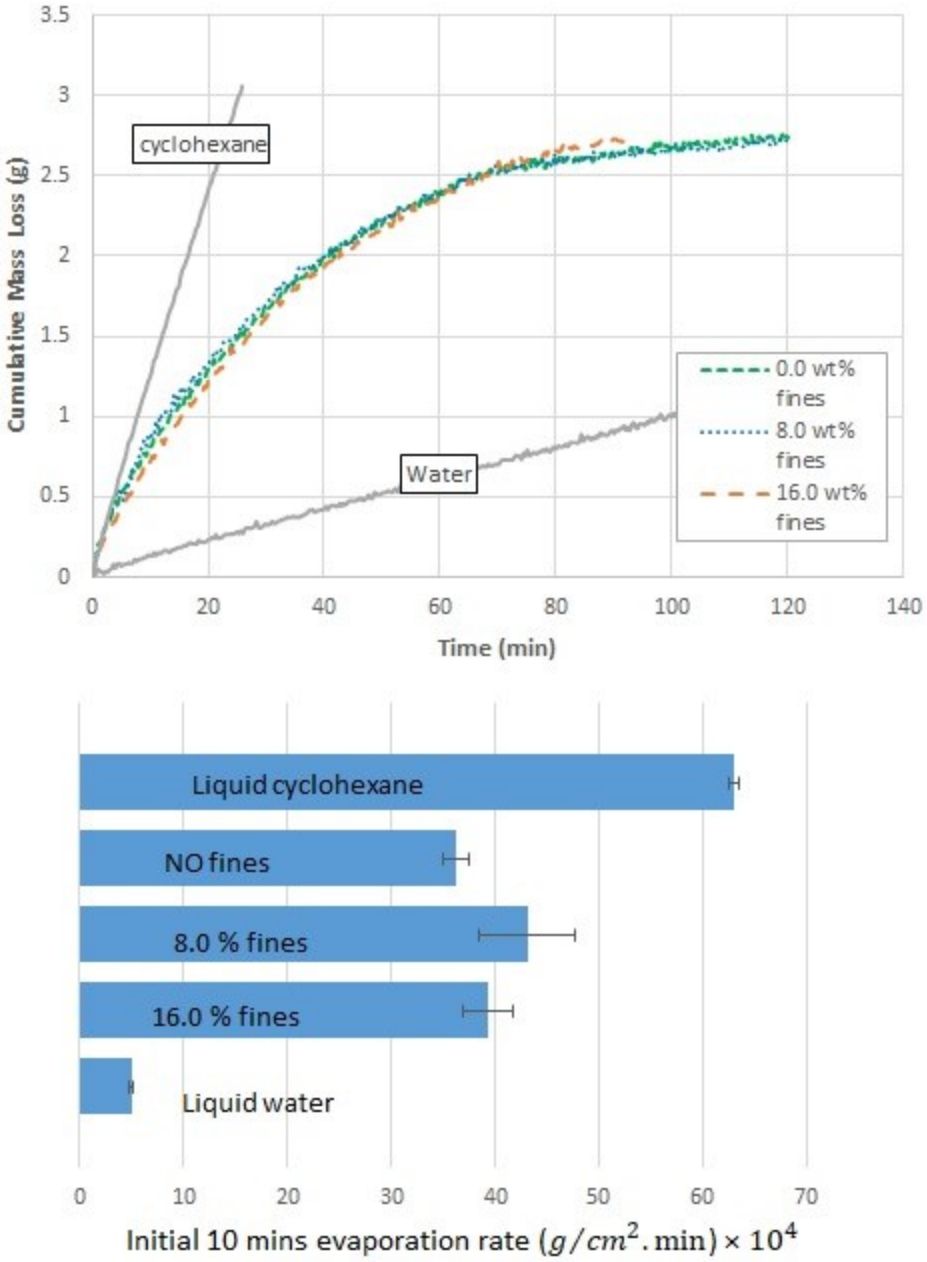

Figure 24 - (top) Drying curves of reconstituted gangue samples with 12 wt% cyclohexane, 3.88 wt% water, 1.0 wt% Bit.C, and 0.0, 8.0, and 16.0 wt% fine solids (bottom) the initial drying flux obtained from the drying curves

4.Discussion

4.1. Formation of Cyclohexane Liquid Film

The liquid film formation occurs in a porous medium when two conditions are met: the solid surface is wetted by the liquid and the capillary forces are much stronger compared to viscous and gravity forces [46], [48], [50], [54]. As will be shown in the following, such two conditions were met in the reconstituted gangue samples prepared in this work and thus, cyclohexane liquid films were formed.

Cyclohexane fully wets soxhlet solids isolated from Alberta oil sands. Panda [47] determined the wettability of soxhlet solids isolated from Alberta rich grade oil sands and compared it to the surface tensions of water, cyclohexane, and bitumen. He reported critical surface tensions of 34 ± 7 and 29-32 ± 5 mN/m for soxhlet solids and DSBS with Bit.C ranging from 0-2 wt%, respectively. This is higher than the surface tension of cyclohexane and much lower than the surface tension of water. He concluded that soxhlet solids are fully wetted by cyclohexane and not by water.

Moreover, this was visually evident as cyclohexane, unlike water, does not form a droplet on soxhlet solids surfaces. Cyclohexane penetrates through such solid surfaces regardless of how compact the surfaces are (even in the case of pellets prepared for contact angle measurements—Figure 16- Schematic (left) and real (right) pictures of the pellets prepared for contact angle measurement). Wetting of solids by cyclohexane compared to that by water is displayed in Figure 25.

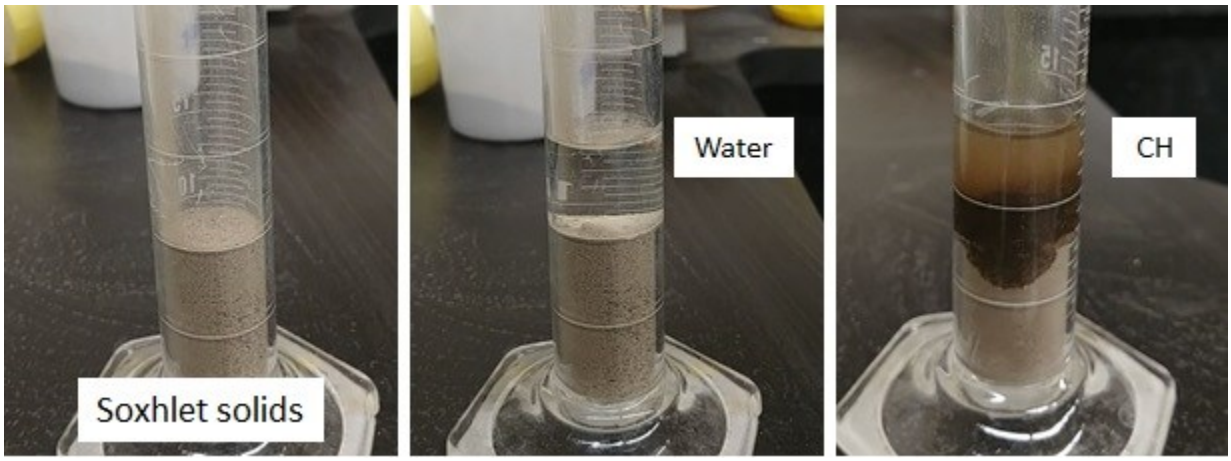

Figure 25- Water does not penetrate soxhlet solids unless mixed vigorously whereas cyclohexane (CH) penetrates the solids upon contact

To probe the dominance of capillary forces, we will do order of magnitude estimations of the capillary and Bond numbers introduced in Section 1.4.1 through equations (7), (12), and (13). The estimations for drying of a square pore channel, saturated with cyclohexane (fully wetting soxhlet solids' surface), are presented in Table 9. Values lower than 0.1 for these numbers indicate the span of liquid films through the whole sample.

For these calculations, we have used orders of magnitude for quantities of which exact values are not known. To obtain the mean value of pore size, an accurate pore size distribution is needed. Here, the pore size has been taken to be in a broad range of 1-100 µm since as mentioned in Section 03.2, the order of magnitude of pore size distribution can be considered roughly monotonic with the particle size distribution. It should be noted that the goal here is to simply verify the negligibility of viscous and gravity forces compared to capillary forces. The values taken for different parameters are presented in Table 10.

As can be seen in Table 9, capillary and Bond numbers reach a maximum order of magnitude of 0.1 for a mean pore size of 1 µm. It should be noted that 1 µm is an unrealistically small pore size

given that more than 90% of solid particles are larger than 45 µm (Table 3). In addition, unlike the "thick" liquid films, we discuss here, "thin" liquid films formed in pores smaller than 1 µm up to a few nanometers have a negligible effect on liquid transport within the pores [46]. Therefore, the formation of liquid films is evident.

Table 9- Estimation of capillary and Bond numbers in a square pore channel with size of r_0 saturated with cyclohexane

Dimensionless number	Description	Equation	Order of magnitude
Capillary number	Specifically defined for a square throat in a 2-D model of porous medium [46]	$Ca = \frac{\pi D C_e \mu_l}{2\alpha \rho_l r_0 \gamma}$ Equation (7)	~10^{-3} for average pore sizes of 100 µm ~10^{-1} for average pore sizes of 1 µm
Capillary number	An estimation of the ratio of pressure differences induced by viscous and capillary forces [50]	$N_{vis} = \frac{\Delta P_{vis}}{P_c} = \frac{\lambda . \beta . e . \mu_l . L}{\rho_l . r_0 . \gamma}$ Equation (12)	
Bond number	An estimation of the ratio of pressure differences induced by gravity and capillary forces [50]	$N_{vis} = \frac{\Delta P_g}{P_c} = \frac{r_0 . \rho_l . g . L}{\lambda . \gamma}$ Equation (14)	

Table 10- Parameters used in the calculation of capillary and Bond numbers shown in Table 9

Parameter	Description	Value/order of magnitude
D	Cyclohexane vapor diffusion coefficient	$2.5 \times 10^{-5}\ m^2/s$
C_e	Equilibrium cyclohexane vapor mass fraction kg/kg	$\sim\frac{P^0_{cyclohexane}}{P^0} \times \frac{M_{cyclohexane}}{V_{m_{air}}} = 0.41\ kg/m^3$
μ_l	Cyclohexane dynamic viscosity	$0.993 \times 10^{-3}\ Pa.s$
α	Shape factor [46]	$\sim 10^{-3}$
ρ_l	Cyclohexane liquid density	$778\ kg/m^3$
r_0	Pore size	$\sim 1 - 100\ \mu m$
γ	Cyclohexane surface tension	$24.6 \times 10^{-3}\ N/m$
λ	Shape factor [50]	3.77
β	Dimensionless resistance [50]	100
e	Evaporation flux	$10^{-3}\ kg/m^2.s$
L	Pore channel length	$1\ cm = 10^{-2} m$
g	Acceleration of gravity	$9.8\ m/s^2$

4.2. Film Flow and Evaporation Fluxes

The initial drying flux is directly correlated to the rate of liquid cyclohexane film flow and that of the evaporation from the surface. At the initial stage of drying, liquid cyclohexane migrates to the surface through liquid film flow and subsequently evaporates at the surface with a high constant rate. It should be noted that we assumed the liquid films in the corners of macro pores are the major liquid transfer mechanism at this stage. As mentioned before, there are also liquid films formed in pores with sizes of a few nanometers of which role in liquid transport is negligible.

Now, we can discuss how liquid film affects the initial drying flux. The drying of cyclohexane at the initial stage, where liquid films of cyclohexane are present, includes two steps (Figure 26):

(i) Transport of liquid cyclohexane through liquid film flow

(ii) Steady state evaporation of cyclohexane from the surface of the sample

It is noteworthy to have an estimation of the rates of these two steps. The evaporation rate of cyclohexane from the surface can be calculated by Equation (11). However, determining the thickness of the diffuse layer (δ) is challenging. Therefore, the mass flux of the second step is experimentally measured and has an order of magnitude of $10^{-3}\ \frac{kg}{m^2.s}$, under the drying conditions used in this study.

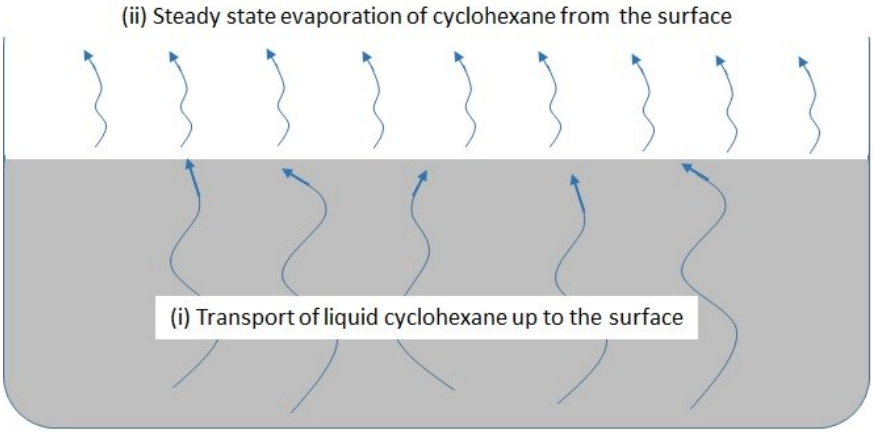

Figure 26- Removal of cyclohexane in the initial stage of drying is a two-step process: (i) liquid cyclohexane migrates up to the surface through liquid film flow (ii) cyclohexane evaporates from surface with a constant rate

The volumetric flow rate of the first step, i.e., the liquid film flow, can be estimated for a square pore channel using Equation (6), as mentioned in Section 1.4.1. In order to have an estimation, we consider a mean mass flux along the channel with the length of L

$$\bar{m}_x = \frac{\rho}{A}.\frac{\int_L^0 Q_x}{L} \approx \frac{\alpha.\rho.\gamma}{\mu_l}.\frac{r_{ave}}{L} \quad (26)$$

In this equation, the area of liquid film has taken to scale with r_0^2. Also, r_{ave} is the mean radius of curvature of the liquid film (Figure 6)

$$r_{ave} = \frac{\int_0^{\frac{r_0}{2}} r.dx}{r_0} \approx f(r_0) \quad (27)$$

and is both a function of and has the same order of magnitude of r_0 , the pore size. We assume here that the radius of curvature can vary from 0 to $\frac{r_0}{2}$. The estimation is presented in Table 11.

Here, r_{ave} has been taken to vary in a range of 1-100 µm (same order of magnitude as the pore size) and L has the order of magnitude of bed height, 1 cm in our case. Values of $\alpha, \gamma, \rho, and\ \mu_l$ are the same as presented in Table 10.

Table 11- Order of magnitude estimates of the film flow and evaporation fluxes

Mass fluxes of the two steps of solvent removal during the initial drying stage ($\frac{kg}{m^2.s}$)	**Equation**	**Order of magnitude**
Liquid film flow rate	$\bar{m}_x \approx \frac{\alpha.\rho.\gamma}{\mu_l}.\frac{r_{ave}}{L}$	10^{-3} for r = 1 µm 10^{-1} for r = 100 µm
Evaporation flux	$e = \rho_g.D.\frac{(c_i - c_\infty)}{\delta}$ (Experimentally measured)	10^{-3}

As can be seen, cyclohexane evaporation flux, being lower than film flow rate, is the limiting factor. We can imagine an equilibrium film thickness at the tip of the film which directly affects the initial drying flux by increasing liquid evaporating surface. This equilibrium film thickness is formed based on the balance between film flow and evaporation. We can obtain a steady state constant initial drying rate as long as film flow rate >> evaporation flux. If evaporation flux is increased, a higher initial drying flux is obtained but for a shorter transition time. In this case, the average film thickness is lower and thus, the liquid film connectivity breaks up in shorter times.

Now we can look at the parameters at play affecting the initial drying and explain the effect of operational and compositional parameters. The evaporation flux is mostly dependent on C_i , the mass fraction of cyclohexane in air near the surface of liquid, which can be directly estimated via vapor pressure

$$C_i = \frac{m_{CH}}{m_{air} + m_{CH}} = \frac{N_{CH}.M_{CH}}{N_{air}.M_{air} + N_{CH}.M_{CH}} \quad (28)$$

Where N_{CH} and N_{air} are moles of cyclohexane in the air close to liquid surface and mole of air, and M_{CH} and M_{air} are molar masses of cyclohexane and air, P_{CH}^0 and P_0 are the vapor pressure of cyclohexane and atmospheric pressure. In this equation, we can estimate the mole fraction of cyclohexane in the air with its vapor pressure in atmospheric pressure. C_i has a value of 0.248 for cyclohexane at 20 °c.

Increasing drying temperature and applying vacuum will increase the evaporation flux by increasing cyclohexane vapor pressure and decreasing atmospheric pressure, respectively. Dissolution of bitumen in cyclohexane in a proportion of 1:12 (based reconstituted gangue composition) does not have a significant effect on cyclohexane vapor pressure, as shown

previously by Panda *et al* [44]. As mentioned in Section 1.3.1, cyclohexane has the highest vapor pressure among the "good" solvents for bitumen extraction. The evaporation flux is also inversely correlated to vapor diffuse layer thickness (δ) which can be shortened by applying forced convection such as blowing air over the sample.

On the other hand, film flow is dependent on several parameters such as the ratio of surface tension over viscosity $\left(\frac{\gamma}{\mu}\right)$, pore shape factor (α), and film's average radius of curvature (r_{ave}) which can be expressed by the mean pore size. It is interesting to note that the inverse correlation of film flow rate to the sample bed height can also be seen through the channel length (L).

4.3. Effect of Bitumen

As mentioned in Section 1.5.1, Panda [44] explained how the presence of only 2 wt% Bit.C can increase the "viscosity" of cyclohexane/bitumen solution by 50% and subsequently, drops the gangue's "sorptivity" by 20% (Equation (16)). Sorptivity is a measure of a porous material's capability in absorbing and transferring a liquid via capillarity. It is interesting to note that the ratio of solvent's surface tension over viscosity in the definition of sorptivity $\left(\frac{\gamma}{\mu}\right)$ also appears in film flow mass flux definition (Equation (26). Therefore, both equations could be used to describe the effect of bitumen on the initial drying flux although neither can quantitatively predict the drop in initial drying rate by increasing bitumen content. Nevertheless, bitumen is a highly viscous liquid and can significantly increase cyclohexane's viscosity even if dissolved even in small amounts.

In addition to decreasing sorptivity, bitumen also contributes significantly to solvent retention leading to higher residual solvent concentration in the gangue by the absorption of cyclohexane [24]. Cyclohexane absorbed by bitumen is quite thermodynamically stable and thus, it takes a long time to desorb under ambient conditions. Noorjahan *et al.* [24] found that the rate of cyclohexane desorption from asphaltenes is much lower (near four orders of magnitude) than its absorption rate and it takes over a month to reach equilibrium. Kislistin and Choi [69] measured the solubility of cyclohexane in bitumen through gravimetric analysis. They reported solubility values lower than 0.01-0.05 g cyclohexane/g bitumen for 20% cyclohexane saturation. However, it should be stressed that even if 1 wt% of bitumen is present in the gangue and it absorbs an amount of cyclohexane equivalent to only 1% of its weight, this translates to a 100 ppm residual cyclohexane.

As a result, residual bitumen in the gangue seems to be the major parameter affecting solvent recovery. However, it should be noted that, for a rich grade ore with 11 wt% bitumen, the concentration of Bit.C in the gangue should not exceed 1.0 wt% (corresponding to a 90% bitumen recovery) as recoveries lower than 95% would make the solvent extraction process not economically viable [16]. Concentrations of 1.5 and 2.0 wt% Bit.C in the gangue correspond to 86% and 82% bitumen recoveries in the extraction process, respectively.

4.4. Effect of Water

By varying the water content, it was observed that the initial drying rate dropped substantially for samples with 12.0 wt% water (or higher). Compared to 12.0 wt% water, the initial drying rate increased significantly when water content was lowered to 6.0 wt% and remained almost the

same when water content was further lowered to 3.88 wt%. Interestingly, the initial drying rate decreased again in the sample with 0.0 wt% water.

We can use a simple visualization to better understand the role of water. A pore with a simple square geometry and partially saturated with a liquid is shown in Figure 27. We assumed an even distribution of the liquid in the pore corners. This is a valid assumption for water since water is added and given 24 hours before adding cyclohexane in our protocol for making reconstituted gangue. This model obviously simplifies the pore situation saturation, given the much more complex pore shape as well as size distribution and network in reality. However, we find it extremely helpful in explaining how water affect the initial drying flux.

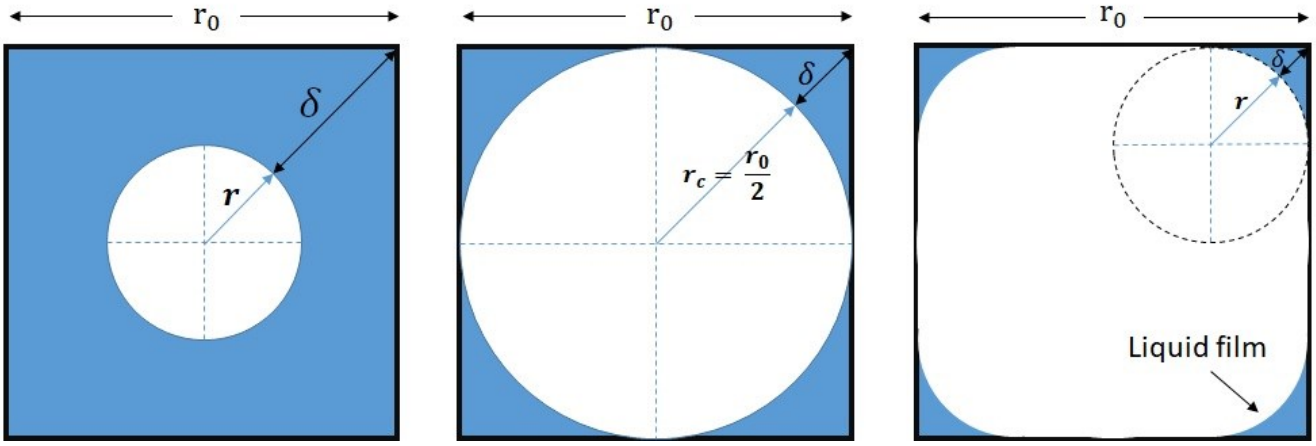

Figure 27- A square pore with a size of r_0: (left) partially saturated with liquid where $\sigma > \sigma_c$ (middle) partially saturated ($\sigma_c = 21\%$) with liquid films on its corners (the liquid film has a radius of curvature $r_c = \frac{r_0}{2}$ and a thickness of $\delta_c = \frac{\sqrt{2}-1}{2}\, r_0$), (right) partially saturated where $\sigma < \sigma_c$) with liquid films on its corners.

Using this model for samples with various water contents (before adding cyclohexane), pore saturation (σ_w) and film thickness of water (δ_w) were calculated and are presented in Table 12. The detailed calculations are presented in 0. In these calculations, the total pore saturation (σ_{total}) was calculated based on a fixed cyclohexane content (12.0 wt% corresponding to a pore

saturation of $\sigma_{CH} = 45.63\ \%$) and bitumen content (1.0 wt% corresponding to a pore saturation of $\sigma_{bit} = 2.96\ \%$). Please note that bitumen is not represented in the model.

Note that at a saturation of 21%, water wets all the solid surface (the middle picture in Figure 27). Therefore, if cyclohexane is added at this level of water saturation (or higher), it will not have access to solid surface and consequently, no cyclohexane liquid film can form. A 21% saturation with water corresponds to 7.1 wt% water in this model. This explains the drop in the initial drying rate at 12.0 wt% and higher amounts. Furthermore, water at high concentrations (higher than 12%) can clog up the pores in the porous network of solids. It should be noted that 12 wt% water in a gangue sample translates to saturating almost 83% of pores volume. This leads to blockage of the pores, entrapment of cyclohexane clusters, breaking up cyclohexane film on solid surface, losing liquid solvent connectivity, and consequently, significantly reducing the initial rate of solvent evaporation.

Table 12 - Pore saturations and film thickness of water at different water contents

Wt% water	σ_w (%)	σ_{total} (%)	$\frac{r_w}{r_0}$	$\frac{\delta_w}{r_0}$
0	0.00	48.13	0.00	0.00
3.88	11.48	59.61	0.37	0.15
6	17.75	65.88	0.45	0.19
8	23.67	71.80	0.49	0.20
10	29.58	77.71	0.47	0.23
12	35.50	83.63	0.45	0.25
15	44.38	92.51	0.42	0.29
17	50.29	98.42	0.40	0.31
20	59.17	107.30	0.36	0.35

On the other hand, we observed that the sample with 0.0 wt% water showed a noticeably lower drying flux compared to samples containing 3.88-6.0 wt% water. To explain this observation, we need to look into water-solid interaction in order to understand how water affects cyclohexane's liquid film.

In reality, water partially wets solids surface. Also, solid surface's hydrophilicity is heterogeneous, i.e., some parts are more hydrophilic than the others due to surface roughness or different surface chemistry. This means that water does not form fully homogenous liquid films on the corners. Nevertheless, water, having a high surface tension, tends to condensate in smaller pores due to Kelvin effects (Equation (14)). Therefore, we can assume that water wets corners of the

pore on spots with higher hydrophilicity. Now, we can discuss why an optimum amount of water might facilitate the formation of liquid cyclohexane films up to the surface of the sample.

Partially wetting of the solid surface by water and reducing the total solid surface available for solid-cyclohexane interactions leads to a thicker liquid film of cyclohexane. This can be seen in Figure 28, where we can compare the cyclohexane liquid film formed in the square pores with and without water. At these low contents of water, we assume that the corners in pores are fully water-wetted. As a result, cyclohexane film will have a higher average thickness through the pore channel, resulting in a stronger liquid film flow of cyclohexane (Equation (26)).

Another interesting change in the sample with no water was weak efflorescence effect (deposition of bitumen on the top layer). It might be suggested that an optimum amount of water also assists dislodging the residual bitumen from the solid surface, hence facilitating its migration to the top of the sample through capillary action. However, this could be explained using film thickness as well. As discussed, cyclohexane liquid film has a lower average thickness in the sample with no water. Lower thickness means shorter time until liquid film connectivity to the top is lost. Thus, there is simply not enough time for bitumen migration to occur. This is verified if bitumen deposition happens in a sample with no water but substantially higher amounts of cyclohexane. An example of this is the preparation of DSBS in Section 2.4 where there is a large amount of cyclohexane in the solids, with no water where it was needed to constantly mix bitumen/cyclohexane solution with solids. The reason was if the mixture is left to dry in the fume hood, a thick layer of bitumen forms on the top, resulting in uneven distribution of bitumen. Moreover, Panda [47] reported higher bitumen deposition ratios for reconstituted gangue samples containing 12 wt% cyclohexane compared to samples with 8 wt% cyclohexane.

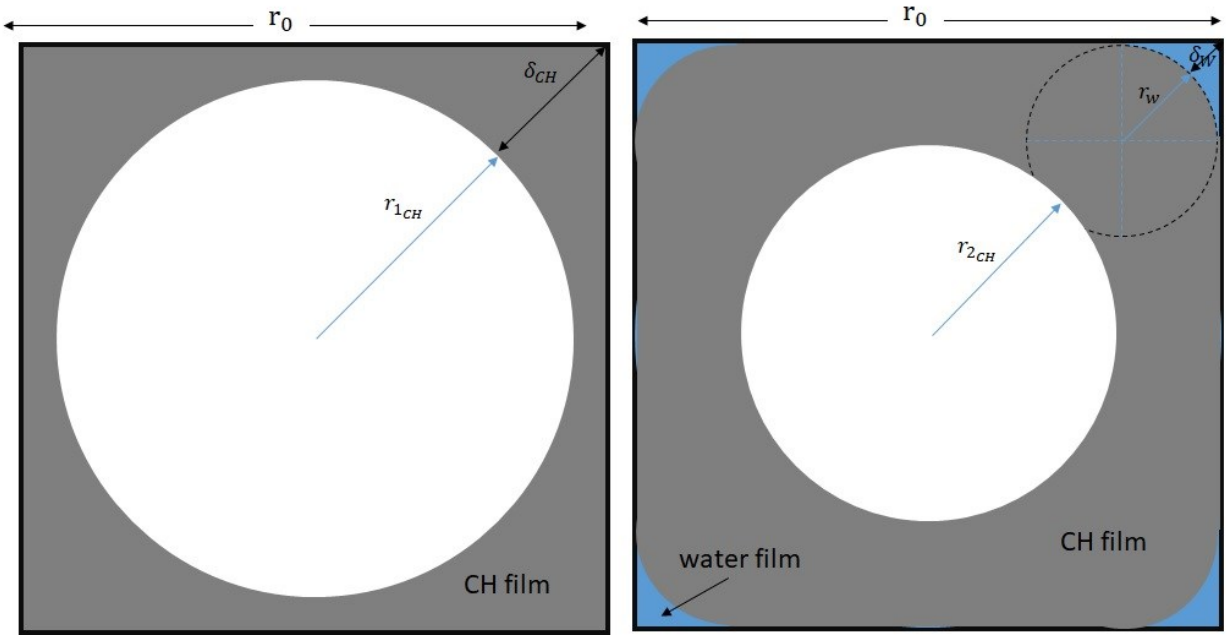

Figure 28 – Liquid film of cyclohexane has lower thickness on average without the presence of water (left) compared to the sample with 3.88 wt% water (right)

4.4.1. Effect of n-Butanol Instead of Water

It was observed that the presence of n-butanol instead of water significantly dropped the initial drying rate. N-butanol is an organic compound and is a cyclohexane-miscible liquid. Thus, analogous to the effect of bitumen on sorptivity, this significant drop may be attributed to the increase in viscosity of cyclohexane/n-butanol mixture compared to that of cyclohexane. However, even the sample with 25 wt% n-butanol, where all the pore volume is saturated with liquid n-butanol/cyclohexane mixture, shows almost the same, low initial drying rate.

Although we could not fully explain this observation, we can conclude that using any organic liquid to "treat" the gangue better remove cyclohexane is not practical. Mixing cyclohexane with any organic liquid with a higher viscosity will result in lower initial drying flux. In addition, adding any other organic liquid (with a vapor pressure probably lower than cyclohexane) to the mixture will add more complexity, i.e., removing a second organic solvent.

4.4.2. Effect of 1 M NaCl Solution

The addition of NaCl to water was inspired by a molecular dynamics simulation study [61]. The equilibrium state of water and cyclohexane was studied between the two octahedral and tetrahedral surfaces of a kaolinite nanoscale pore. It was observed that adding 1 M of Na^+ and Cl^- ions to the aqueous phase resulted in a complete wetting of the basal surfaces by water and thus, a complete desorption of cyclohexane from the solid surfaces. This impact of ions was explained by the shortening the decay length and modifying the surface potentials.

However, replacing water with NaCl solution had almost no effect on the drying. This might be related to the scale of the two studies. The pore size in the simulation is in nano scale while in our study, the macroscopic drying of a porous medium, thin films of liquid film having a thickness of a few nanometers do not play a major role.

4.5. Effect of Fines

It was observed that variation of fines did not have a significant impact on the initial drying rate. This was rather unexpected since both porosity (Table 2) and hydrophobicity (

Table 6) changed with increasing amount of fines. This could be due to the two offsetting effects of increasing fines.

Increasing fines enhances hydrophobicity which is in favor of liquid film flow. It should be noted that γ in Equation (5) is actually $\gamma \times \cos(\theta)$, representing surface interaction of cyclohexane on solid surface ($\gamma_{solid} - \gamma_{solid/CH}) \times \cos(\theta)$ does not appear in the equation because θ has been taken to be zero in the derivation.

On the other hand, increasing the fines content decreases mean pore size of the solids which weakens film flow rate. This may sound counter-intuitive that a larger radius is favorable to capillary flow while we know for a fact that capillary pressure has an inverse correlation with radius of curvature. Capillary pressure is an indicator of how strong capillary forces are and eventually dictates how "high" the liquid meniscus can go in a capillary against viscous and gravity forces. The well-known example is the height of meniscus in a capillary which is determined by balancing capillary force against gravity:

$$h = \frac{2\gamma\cos(\theta)}{\rho g r} \tag{29}$$

This number for cyclohexane in a capillary with $r = 100\ \mu m$ and $\theta = 0$, is 6.34 cm , far beyond the bed height in gangue samples. However, when discussing "flow flux," we are referring to how "fast" the meniscus moves in a capillary. Here, the flux is directly correlated to the radius of curvature (which itself is related to pore size). The well-known Washburn equation is a good example, describing the motion of a meniscus in a simple cylindrical capillary of radius r (compare to Equation (28)):

$$x(t) = \sqrt{\frac{\gamma r t}{2\mu}} \tag{30}$$

5.Conclusions

Drying of porous media such as the solvent-extracted gangue displays two stages: an initial stage with a fast, linear drying rate, and a final stage with a significantly slower, constant rate. Solvent liquid film flow, formed in the corners of the pores, is the major drying mechanism in the initial stage. The liquid solvent, which fully wets the gangue solids surfaces, is transferred through film flow to the open end of the sample bed and subsequently, evaporates with a constant rate close to that of the free evaporation in its liquid state. As long as solvent's liquid connectivity throughout the sample exists, the film flow pumps solvent up to the surface where it can evaporate with a rate of free liquid evaporation. As a result, the initial stage of drying is dominated by the evaporation of solvent and has the major significance in more efficient removal of the solvent under ambient conditions.

Drying at the initial stage consists of two processes: film flow and surface evaporation. As long as film flow rate >> evaporation flux, liquid film spans throughout the sample and a constant rate of drying, limited by evaporation flux, is achieved. The effect of any operational or compositional parameter on the initial drying rate can be explained through its effect on film flow and evaporation fluxes. The film flow rate is directly correlated to pore shape and geometry, liquid's density, liquid's affinity to solid surfaces, and the average pore size while it is inversely correlated to liquid's dynamic viscosity and the pore channel length which is a representation of bed height. Evaporation flux is mainly dependent on the vapor pressure of the liquid and also inversely correlated to the vapor's diffuse layer which can be shortened by applying forced convection.

In this study, reconstituted gangue samples with controlled compositions were prepared, mimicking cyclohexane-extracted gangue. While a fixed 12 wt% of cyclohexane was added to all samples, bitumen, water, and fines contents varied and their effects on the initial drying rates of the samples were observed. The effect of each component on the initial drying rate can be explained by their effect on the film flow rate. The goal was to investigate how much the composition of the gangue, originating from the original ore's composition, would affect gangue's drying.

Bitumen, even in an amount as small as 2% in the gangue, significantly reduces the initial drying rate by substantially increasing cyclohexane viscosity. Bitumen can also contribute to solvent retention to a great amount by stable adsorbing of cyclohexane.

An optimum amount of water, i.e., 3.88-6 wt%, was found to result in high initial drying rates. Water in higher amounts such as 12 wt%, covers the entire gangue solids surfaces, not allowing for cyclohexane liquid films to form. In addition, high water contents can result in the blockage of pores and entrapment of cyclohexane. On the other hand, completely removing water from the gangue leads to a thinner cyclohexane liquid film and consequently a lower initial drying rate. Adding NaCl to water did not show to have any effects on drying. Moreover, replacing water with n-butanol led to noticeably slow initial drying rates, in all n-butanol contents from 3.88-25 wt%.

Fines content variation showed no significant effect on drying. This was attributed to two different effects of increasing fines which might offset each other. Increasing the amount of fines contributes to lowering the average pore size which reduces the film flow rate. On the other hand, due to asphaltenes precipitation on fines surfaces, they have much higher carbon content

compared to coarse solids. Thus, increasing fines enhanced solids hydrophobicity and affinity to solvent.

5.1. Industrial Implications

Cyclohexane has been recommended as a suitable solvent for NAE. In addition to having shown an acceptable extraction performance, cyclohexane is also volatile enough to be optimally recovered from the gangue.

Applying heat or vacuum does not greatly improve the film flow and the initial drying rate. Increasing temperature affects several parameters including elevating solvent's vapor pressure and consequently, the evaporation flux. However, increasing temperature has minor effects on film flow rate, compared to its noticeable effect on diffusion-dominated evaporation flux. Moreover, applying vacuum also increases evaporation flux but has no effect on the film flow rate.

Our theoretical explanation of lower sensitivity of the initial drying stage of the gangue to applying temperature and vacuum (compared to the final stage of drying), is in agreement with a previous experimental study [55]. As shown in Figure 10 (top), by increasing samples temperature from 25 °c to 95 °c, the time of initial drying stage (reaching 2 from 12 wt% cyclohexane) decreases from ~46 to ~10 minutes while the time of final drying stage (reaching 250 ppm from 2 wt% cyclohexane) decreases from ~80 to ~1 minute.

According to 0, NAE would be as energy intensive as water-based extraction if solvent is to be removed by heating up the sample from the beginning. However, this is not necessary. Due to the presence of film flow, the initial drying stage is fast at ambient conditions. Therefore, any

external energy input by applying harsher operational conditions, i.e. raising temperature or applying vacuum, for better removal of solvent from the gangue can be avoided until the initial drying stage is over. After the initial stage is over, only ~20% of the energy calculated in Appendix B is needed since more than 80% of cyclohexane is removed.

Moreover, it should be stressed that all the results reported above were measured for samples with bed heights of 1 cm. The significant impact of bed height on drying of the gangue has been shown experimentally in [47] and discussed theoretically in this work. Decreasing bed height can also be highly profitable as it substantially decreases the final residual cyclohexane in the gangue.

On the other hand, compositional parameters of the gangue should be controlled in order to achieve more efficient drying. Decreasing residual bitumen content significantly improves the initial drying rate and minimizes the final content of the residual solvent. Therefore, it is recommended to focus on further improving the extraction performance in NAE methods. Controlling water content in an optimum range helps minimize the adverse effects of high and very low water contents. Water content in poor grade ores containing high amounts of water is better to be reduced to the optimum range before feeding to extraction units. Fines content does not have any significant effect on the initial drying rate. However, they may adversely affect the extraction performance, leading to higher residual bitumen in the gangue, and thus impair the optimum removal of solvent from the gangue.

5.2. Future Work

- The role of particle and pore size distribution was not thoroughly investigated in this work due the lack of rigorous measurement methods. Obtaining pore and particle size

distributions of the solids sample using rigorous methods such as liquid saturation and dynamic light scattering will help shed more light on the role of the two parameters on drying.

- The interaction between the variables in this work can also be investigated. For example, it is suggested to investigate the role of fines on gangue's drying, at different bitumen contents.
- As the major parameters at play for drying of the gangue have been detected, an empirical model can be developed in order to predict the drying behavior of the gangue in different conditions. Using such model, a drying process can be modified for different gangue compositions and/or different operational parameters.
- The major issue with heating up the gangue is the excessive amount of energy needed to heat the whole sample, i.e. the solids, water, and the residual bitumen along with the residual solvent. Therefore, the use of a selective method for only heating up the solvent, such as microwave heating, seems interesting.

References

[1] G. of Alberta, “Oil sands facts and statistics | Alberta.ca.” [Online]. Available: https://www.alberta.ca/oil-sands-facts-and-statistics.aspx. [Accessed: 26-Apr-2019].

[2] J. H. Masliyah, J. Czarnecki, and Z. Xu, “Handbook on Theory and Practice of Bitumen Recovery from Athabasca Oil Sands Volume I,” in *Handbook on Theory and Practice of Bitumen Recovery from Athabasca Oil Sands Volume I*, vol. 1, Kingsley Knowledge Pub, 2011, pp. 173–256.

[3] Government of Alberta, “Talk about SAGD,” 2013.

[4] Government of Alberta, “Oil Sands Facts and Stats,” 2017.

[5] “Oil Sands Operations | Oil Sands Magazine.” [Online]. Available: https://www.oilsandsmagazine.com/projects/bitumen-production#Chart. [Accessed: 26-Apr-2019].

[6] “Regional Aquatics Monitoring Program (RAMP).” [Online]. Available: http://www.ramp-alberta.org/resources/development/history/insitu.aspx. [Accessed: 26-Apr-2019].

[7] “Canada Oil Sands Project | JAPEX.” [Online]. Available: https://www.japex.co.jp/english/business/ep_o/canada_oilsands.html. [Accessed: 19-Dec-2019].

[8] “CERA Oil Sands, Greenhouse Gases, and US Oil Supply Getting the Numbers Right Special RepoRt ™,” 2010.

[9] S. Gupta, S. Gittins, and P. Picherack, “Field Implementation of Solvent Aided Process,” in *Canadian International Petroleum Conference*, 2002.

[10] F. Lin, S. R. Stoyanov, and Y. Xu, “Recent Advances in Nonaqueous Extraction of Bitumen from Mineable Oil Sands: A Review,” *Org. Process Res. Dev.*, vol. 21, no. 4, pp. 492–510, 2017.

[11] H. Zhao, T. Dang-Vu, J. Long, Z. Xu, and J. H. Masliyah, “Role of Bicarbonate Ions in Oil Sands Extraction Systems with a Poor Processing Ore,” *J. Dispers. Sci. Technol.*, vol. 30, no. 6, pp. 809–822, May 2009.

[12] Alberta Energy Regulator, “Alberta’s Energy Reserves 2011 and Supply/Demand Outlook 2014–2021,” p. 299, 2015.

[13] S. E. Hrudey *et al.*, “The Royal Society of Canada Expert Panel: Environmental and Health Impacts of Canada’s Oil Sands Industry: Report,” *Engineering*, no. December, p. 22, 2010.

[14] E. Canada, “Canada ’ S Emissions Trends,” *Environment*, no. July, pp. 1–60, 2011.

[15] H. Sui, G. Ma, L. He, Z. Zhang, and X. Li, “Recovery of Heavy Hydrocarbons from Indonesian Carbonate Asphalt Rocks. Part 1: Solvent Extraction, Particle Sedimentation, and Solvent Recycling,” 2016.

[16] H. Nikakhtari, L. Vagi, P. Choi, Q. Liu, and M. R. Gray, “Solvent screening for non-aqueous extraction of Alberta oil sands,” *Can. J. Chem. Eng.*, vol. 91, no. 6, pp. 1153–1160, 2013.

[17] P. O. Redelius, “Solubility parameters and bitumen,” *Fuel*, vol. 79, no. 1, pp. 27–35, 2000.

[18] J. M. Kenchington and C. R. Phillips, “Operating Cost Parameters in Solvent Extraction of Bitumen from Oil Sand Mineral Deposits,” *Energy Sources*, vol. 5, no. 4, pp. 317–338, Jan. 1981.

[19] X. Li, L. He, G. Wu, W. Sun, H. Li, and H. Sui, “Operational Parameters, Evaluation Methods, And Fundamental Mechanisms: Aspects of Nonaqueous Extraction of Bitumen from Oil Sands,” *Energy & Fuels*, vol. 26, no. 6, pp. 3553–3563, Jun. 2012.

[20] H. Nikakhtari, S. Wolf, P. Choi, Q. Liu, and M. R. Gray, “Migration of fine solids into product bitumen from solvent extraction of Alberta oilsands,” *Energy and Fuels*, vol. 28, no. 5, pp. 2925–2932, 2014.

[21] J. H. Hildebrand and 1881-, “Solubility of non-electrolytes.” Reinhold Pub., 1936.

[22] I. Rahimian and G. Zenke, “ZUM VERHALTEN ORGANISCHER LOESEMITTEL GEGENUEBER BITUMEN,” *BITUMEN*, vol. 48, no. 1, 1986.

[23] C. M. Hansen, *Hansen Solubility Parameter: a user’s handbook*. CRC Press, 2002.

[24] A. Noorjahan, X. Tan, Q. Liu, M. R. Gray, and P. Choi, “Study of cyclohexane diffusion in athabasca asphaltenes,” *Energy and Fuels*, vol. 28, no. 2, pp. 1004–1011, 2014.

[25] E. P. Guymon, “SOLVENT AND WATER/SURFACTANT PROCESS FOR REMOVAL OF BITUMEN FROM TAR SANDS CONTAMINATED WITH CLAY,” Canadian Patent No. 2024519, 1996.

[26] L. Mirmontazeri, S. Afshar, and A. Yeung, “Evaluation of naphthenic acids as a soil remediation agent: A physicochemical perspective,” *Fuel*, vol. 128, pp. 1–6, Jul. 2014.

[27] S. Afshar, L. Mirmontazeri, and A. Yeung, “Potential use of naphthenic acids in soil remediation: Examination of pore-scale interfacial properties,” *Fuel*, vol. 116, pp. 395–398, 2014.

[28] W. Liu, Y. Jin, X. Tan, and A. Yeung, “Altering the wettability of bitumen-treated glass surfaces with ionic surfactants,” *Fuel*, vol. 90, no. 9, pp. 2858–2862, Sep. 2011.

[29] J. Duyvesteyn, W. P. C.; Kift, “Dry, stackable tailings and methods for producing the same,” U.S. Patent No. 8257580, 2012.

[30] G. Wu, X. A.; Jones, G. B.; Cymerman, “Extraction of oil sand bitumen with two solvents,” U.S. Patent No. 8858786, 2014.

[31] C. M. Duyvesteyn, W. P. C.; Joshi, M.; Kift, J.; Zelnik, D. J.; Thompson, W. C.; Hoffman, “Methods for extracting bitumen from bituminous material,” U.S. Patent No. 8877044, 2014.

[32] S. Gan, E. V. Lau, and H. K. Ng, “Remediation of soils contaminated with polycyclic aromatic hydrocarbons (PAHs),” *J. Hazard. Mater.*, vol. 172, no. 2–3, pp. 532–549, 2009.

[33] D. H. Lee, R. D. Cody, D. J. Kim, and S. Choi, “Effect of soil texture on surfactant-based remediation of hydrophobic organic-contaminated soil,” *Environ. Int.*, vol. 27, no. 8, pp. 681–688, 2002.

[34] A. Silva, C. Delerue-Matos, and A. Fiúza, “Use of solvent extraction to remediate soils contaminated with hydrocarbons,” *J. Hazard. Mater.*, vol. 124, no. 1–3, pp. 224–229, 2005.

[35] R. Khalladi, O. Benhabiles, F. Bentahar, and N. Moulai-Mostefa, “Surfactant remediation of diesel fuel polluted soil,” *J. Hazard. Mater.*, vol. 164, no. 2–3, pp. 1179–1184, 2009.

[36] E. R. Gable, C. M.; Duncan, E. A. J.; Freitas, “Selective Solvent Extraction Plus Filtration of Tar Sands,” U.S. Patent No. 3475318, 1969.

[37] R. L. Mehlberg, “Method for stripping of residual solvent,” U.S. Patent No. 4802975, 1989.

[38] S. Wu, X. A.; Bhattacharya, “Process for recovering solvent from spent oil sand solids,” 8552244, 2013.

[39] J. Funk, E. W.; Major, W. G.; Pirkle, J. C., “Solvent extraction process for tar sands,” U.S. Patent No. 4347118, 1982.

[40] W. C. Kift, J.; Joshi, M.; Hoffman, C.; Thompson, “Process for extracting bitumen and drying the tailings,” U.S. Patent No. 8968556, 2012.

[41] S. A. Brough, S. H. Riley, G. S. McGrady, S. Tanhawiriyakul, L. Romero-Zerón, and C. D. Willson, “Low temperature extraction and upgrading of oil sands and bitumen in supercritical fluid mixtures,” *Chem. Commun.*, vol. 46, no. 27, pp. 4923–4925, 2010.

[42] H. Nikakhtari, K. Pal, S. Wolf, P. Choi, Q. Liu, and M. R. Gray, “Solvent Removal from Cyclohexane-Extracted Oil Sands Gangue,” vol. 94, no. January, pp. 408–414, 2016.

[43] “Cyclohexane | C6H12 - PubChem.” [Online]. Available: https://pubchem.ncbi.nlm.nih.gov/compound/Cyclohexane. [Accessed: 01-Nov-2019].

[44] S. Panda, K. Pal, S. Merzara, M. R. Gray, Q. Liu, and P. Choi, “Transport and removal of a solvent in porous media in the presence of bitumen, a highly viscous solute,” *Chem. Eng. Sci.*, vol. 165, pp. 229–239, 2017.

[45] Y. C. Yortsos and A. K. Stubos, “Phase change in porous media,” *Curr. Opin. Colloid Interface Sci.*, vol. 6, no. 3, pp. 208–216, 2001.

[46] A. G. Yiotis, A. G. Boudouvis, A. K. Stubos, I. N. Tsimpanogiannis, and Y. C. Yortsos, “Effect of liquid films on the drying of porous media,” *AIChE J.*, vol. 50, no. 11, pp. 2721–2737, 2004.

[47] S. Panda, “Role of Residual Bitumen on the Solvent Removal from Alberta Oil Sands Gangue,” 2015.

[48] M. Prat, “On the influence of pore shape, contact angle and film flows on drying of capillary porous media,” *Int. J. Heat Mass Transf.*, vol. 50, no. 7–8, pp. 1455–1468, 2007.

[49] K. S. Breuer, “IMECE2003-44135,” 2003.

[50] B. Camassel, N. Sghaier, M. Prat, and S. Ben Nasrallah, “Evaporation in a capillary tube of square cross-section: Application to ion transport,” *Chem. Eng. Sci.*, vol. 60, no. 3, pp. 815–826, 2005.

[51] H. Eloukabi, N. Sghaier, S. Ben Nasrallah, and M. Prat, “Experimental study of the effect of sodium chloride on drying of porous media: The crusty-patchy efflorescence transition,” *Int. J. Heat Mass Transf.*, vol. 56, no. 1–2, pp. 80–93, 2013.

[52] N. Sghaier, M. Prat, and S. Ben Nasrallah, “On the influence of sodium chloride concentration on equilibrium contact angle,” *Chem. Eng. J.*, vol. 122, no. 1–2, pp. 47–53, 2006.

[53] N. Shokri, “Pore-scale dynamics of salt transport and distribution in drying porous media,” *Phys. Fluids*, vol. 26, no. 1, 2014.

[54] N. Sghaier and M. Prat, “Effect of efflorescence formation on drying kinetics of porous media,” *Transp. Porous Media*, vol. 80, no. 3, pp. 441–454, 2009.

[55] R. Renaud, “A Study on the Effect of Temperature and Pressure on the Removal of Cyclohexane from Non-Aqueous Extraction Gangue,” 2015.

[56] V. Brito and T. Diaz Gonçalves, “Drying Kinetics of Porous Stones in the Presence of NaCl and $$\hbox {NaNO}_{3}$$ NaNO 3 : Experimental Assessment of the Factors Affecting Liquid and Vapour Transport,” *Transp. Porous Media*, vol. 100, no. 2, pp. 193–210, Nov. 2013.

[57] A. G. Yiotis, I. N. Tsimpanogiannis, A. K. Stubos, and Y. C. Yortsos, “Coupling between external and internal mass transfer during drying of a porous medium,” *Water Resour. Res.*, vol. 43, no. 6, Jun. 2007.

[58] C. Hall, W. Hoff, and W. D. Hoff, *Water Transport in Brick, Stone and Concrete*. CRC Press, 2011.

[59] J. R. Phillip, “The Theory of Infiltration : 4. Sorptivity and Algebraic Infiltration Equations,” *Soil Sci.*, vol. 84, no. 3, pp. 257–264, 1957.

[60] L. I. Ejike, “Role of Fine Solids in Solvent Recovery from Reconstituted Alberta Oil Sands Gangue,” 2016.

[61] M. H. Anvari and P. Choi, “Salt-Induced Phase Separation of Water and Cyclohexane within a Kaolinite Nanopore: A Molecular Dynamics Study,” *J. Phys. Chem. C*, vol. 122, no. 42, pp. 24215–24225, 2018.

[62] “Handbook of Chemistry and Physics 100th Edition.” [Online]. Available: http://hbcponline.com/faces/contents/InteractiveTable.xhtml. [Accessed: 10-Nov-2019].

[63] T. Young, “III. An essay on the cohesion of fluids.,” *Philos. Trans. R. Soc. London*, vol. 95, pp. 65–87, 1805.

[64] H. Huang, “The Mechanism of Floc Formation by Hydrodynamic Cavitation and Its Application on Fine Particle Flotation.”

[65] T. Dang-Vu, R. Jha, S. Y. Wu, D. D. Tannant, J. Masliyah, and Z. Xu, “Wettability determination of solids isolated from oil sands,” *Colloids Surfaces A Physicochem. Eng. Asp.*, vol. 337, no. 1–3, pp. 80–90, 2009.

[66] B. D. Cassie, “Of porous surfaces,” no. 5, pp. 546–551, 1944.

[67] R. Lal, K. Cameron, and G. Buchan, “Porosity and Pore Size Distribution,” *Encycl. Soil Sci. Second Ed.*, pp. 295–303, 2005.

[68] K. Pal *et al.*, “Performance of Solvent Mixtures for Non-aqueous Extraction of Alberta Oil Sands,” *Energy & Fuels*, vol. 29, no. 4, pp. 2261–2267, Apr. 2015.

[69] V. Kislistin and P. Choi, “Thickness Dependence of the Diffusivity and Solubility of Cyclohexane in Nanoscale Bitumen Films,” *ACS Omega*, 2019.

Appendix A: Energy efficiency of water-based vs solvent-based extractions

High energy consumption of the hot water extraction method is one of the main reasons for recently renewed interest in the solvent-based extraction method. On average, the hot water extraction method consumes 1.3 GJ, including energy used for extraction as well as upgrading, to produce 1 barrel of bitumen [2]. This is approximately equal to 22% of the chemical energy stored in a barrel of bitumen. The solvent-based extraction method offers a promising replacement for the water-based extraction method since it can be performed at ambient conditions while yielding high extraction rates. The main challenge is the removal of residual solvent in the gangue after extraction. Heating up the gangue to elevated temperature is not a feasible for solvent removal, since it goes against the very reason for the favorability of solvent-based extraction. However, in this section, we present rough estimations on the energy efficiencies of both water-based and solvent-based extraction methods.

Our assumptions for these calculations are:

- A rich grade ore similar to the one used in this study containing 11 wt% bitumen, 3 wt% water, and 84 wt% solids
- A 95% bitumen recovery rate for both methods
- A gangue composition similar to that of this study, i.e. 1 wt% bitumen, 12 wt% cyclohexane, and 3.88 wt% water, based on dry solids. This composition translates to 85.5 wt% solids, 0.85 wt% residual bitumen, 10.27 wt% residual cyclohexane, and 3.32 wt% water in the gangue

- The solvent in solvent-based extraction is cyclohexane
- The values considered are presented in the table below

Water heat capacity ($\frac{J}{kg\,^\circ c}$)	4186
Solids heat capacity ($\frac{J}{kg\,^\circ c}$) from [2]	800
Bitumen heat capacity ($\frac{J}{kg\,^\circ c}$) from [2]	1800
Bitumen density[1] ($\frac{kg}{m^3}$) from [2]	1000
Cyclohexane heat capacity ($\frac{J}{kg\,^\circ c}$)	1853.6
Cyclohexane heat of vaporization ($\frac{J}{kg}$)	3.69×10^5

- **Water-based extraction**

  First, we look into the energy consumption for extracting 1 barrel of bitumen using water-based method. To produce one barrel of bitumen

  $1\ bbl\ bit \times \frac{0.159\ m^3}{1\ bbl} \times \frac{1000\ kg\ bit}{1\ m^3\ bit} \times \frac{1 kg\ ore}{0.11 \times 0.95\ kg\ bit}$ ~ 1521 kg oil sands ore

  is needed. For each kg of ore ~ 0.5 kg water is mixed. Therefore, for each barrel of bitumen, almost 760 kg water is heated up and mixed with the ore to prepare slurry. Water is usually heated up to 50-90 °C to achieve the operation temperature of slurry preparation. We

[1] Bitumen density varies in a range of 950-1050 $\frac{kg}{m^3}$, based on its hydrogen, nitrogen, and sulfur content [2]. We considered a bitumen density of 1000 $\frac{kg}{m^3}$ in this work.

assume an average of 70 °C for water's operation temperature. The processing water temperature is also assumed to be 20 °C. The energy needed to heat up the water is simply

$$760 \text{ kg water } \times 4186 \frac{J}{kg\ water\ ^\circ c} \times 50\ ^\circ\text{C} = 159.07 \text{ MJ}$$

- **Solvent-based extraction**

Now, let us look at the energy consumption to treat the cyclohexane-extracted gangue. The average heat capacity ($\frac{J}{kg\ ^\circ c}$) of the gangue is

$$0.855 \times 800 + 0.0085 \times 1800 + 0.1027 \times 1853.6 + 0.0332 \times 4186 = 1028.64$$

To produce 1 bbl of bitumen, 1521 kg oil sands ore is needed. The weight of the remaining gangue is almost the same since bitumen (11 wt%) is almost replaced by cyclohexane (12 wt%). We assume heating up the gangue from 20 °C to 81 °C, the boiling temperature of cyclohexane. It should be noted that this is an underestimation as cyclohexane's boiling point in the pores is higher than 81 °C.[2]

$$1521 \text{ kg gangue } \times 1028.64 \frac{J}{kg\ gangue\ ^\circ c} \times 61\ ^\circ\text{C} \sim 95.43 \text{ MJ}$$

Also, the energy needed to vaporize the cyclohexane in the gangue is

$$1521 \text{ kg gangue } \times \frac{0.12\ kg\ cyclohexane}{1\ kg\ gangue} \times \frac{3.69 \times 10^5\ J}{kg\ cyclohexane} \sim 67.3 \text{ MJ}$$

[2] We can have an example of water to have an estimation of how much the boiling temperature changes with surface curvature. Boiling temperature of a water increases to 121°c in a 1μm meniscus at 1atm.

In total, ~163 MJ is needed which is almost the same energy consumption as the water-based method.

Appendix B: Pore saturation calculations

In this section, we present the calculations for pore saturations with water and cyclohexane, which led to the results in Table 11. We consider the bulk volume of M_s g of soxhlet solids to be

$$V_{bulk} = \frac{M_s}{\rho_{bulk}} \tag{31}$$

Porosity is defined as the fraction of pore volume to the bulk volume of the sample[58]. Therefore, pore volume can be calculated as

$$V_{pore} = V_{bulk} \cdot \phi = \frac{M_s \cdot \phi}{\rho_{bulk}} \tag{32}$$

Now, knowing water (ω_w), cyclohexane (ω_{CH}), and bitumen (ω_{Bit}) content (based on dry soxhlet solids), each component's volume and consequently, each component's pore saturation (σ_A , the percentage of pore volume occupied by a component) can also be determined

$$\frac{\sigma_A}{100} = \frac{V_A}{V_{pore}} = \frac{M_A}{V_{pore} \cdot \rho_A} = \frac{\omega_A \cdot M_s}{V_{pore} \cdot \rho_A} = \frac{\omega_A \cdot \rho_{bulk}}{\phi \cdot \rho_A} \tag{33}$$

Where V_A , M_A , and ρ_A are respectively the volume occupied by, mass, and the density of component A. The values taken for each component are presented in Table 13.

Table 13 – The values for pore saturation calculations

A	ω_A	ρ_A ($\frac{g}{cm^3}$)	ρ_{bulk}	ϕ
Water	Ranging from 0 to 20	1	1.42 from Table 2	0.48 from Table 2
Cyclohexane	12.0	0.778		
Bitumen	1.0	1 from [2]		

Later, we can use the pore saturation in the visualized model (i.e., Figure 27- A square pore with a size of r_0: (left) partially saturated with liquid where $\sigma > \sigma_c$ (middle) partially saturated ($\sigma_c = 21\%$) with liquid films on its corners (the liquid film has a radius of curvature $r_c = \frac{r_0}{2}$ and a thickness of $\delta_c = \frac{\sqrt{2}-1}{2} r0$), (right) partially saturated where $\sigma < \sigma c$) with liquid films on its corners.) to calculate liquid film's thickness and radius of curvature. Here, a critical saturation ($\sigma_c = 1 - \frac{\pi r_c^2}{r_0^2}$) based on a critical radius of curvature ($r_c = \frac{r_0}{2}$) is defined where the liquid starts to fully cover solid pore's surface (i.e., the middle picture of Figure 27)

$$\sigma_c = 1 - \frac{\pi r_c^2}{r_0^2} = 1 - \frac{\pi}{4} = 0.215 \tag{34}$$

Pore saturation is simply equal to the ratio of the area of the cross section occupied by the liquid to the total area of pore cross section. Therefore, when $\sigma_c < \sigma < 1$ (i.e., the left picture in Figure 27),

$$\sigma = \frac{r_0^2 - \pi r^2}{r_0^2} \tag{35}$$

and the ratio of radius of curvature to pore size is

$$\frac{r}{r_0} = \left[\frac{1-\sigma}{\pi}\right]^{\frac{1}{2}} \quad for \quad \sigma_c < \sigma < 1 \tag{36}$$

and when $0 < \sigma < \sigma_c$ (i.e., the right picture in Figure 27)

$$\sigma = \frac{4 \times \left[\frac{(2r)^2 - \pi r^2}{4}\right]}{r_0^2} \tag{37}$$

So the ratio of radius of curvature to the pore size

$$\frac{r}{r_0} = \left[\frac{\sigma}{4 - \pi}\right]^{\frac{1}{2}} \quad for \quad 0 < \sigma < \sigma_c \tag{38}$$

Also, the ratio of liquid film's thickness to pore size is simply

$$\frac{\delta}{r_0} = \frac{\sqrt{2}}{2} - \frac{r}{r_0} \tag{39}$$